


Direct observation of coordinated assembly of individual native centromeric nucleosomes

Andrew R Popchock¹, Joshua D Larson², Julien Dubrulle³, Charles L Asbury²  & Sue Biggins^{1,*} 

Abstract

Eukaryotic chromosome segregation requires the kinetochore, a megadalton-sized machine that forms on specialized centromeric chromatin containing CENP-A, a histone H3 variant. CENP-A deposition requires a chaperone protein HJURP that targets it to the centromere, but it has remained unclear whether HJURP has additional functions beyond CENP-A targeting and why high AT DNA content, which disfavors nucleosome assembly, is widely conserved at centromeres. To overcome the difficulties of studying nucleosome formation *in vivo*, we developed a microscopy assay that enables direct observation of *de novo* centromeric nucleosome recruitment and maintenance with single molecule resolution. Using this assay, we discover that CENP-A can arrive at centromeres without its dedicated centromere-specific chaperone HJURP, but stable incorporation depends on HJURP and additional DNA-binding proteins of the inner kinetochore. We also show that homopolymer AT runs in the yeast centromeres are essential for efficient CENP-A deposition. Together, our findings reveal requirements for stable nucleosome formation and provide a foundation for further studies of the assembly and dynamics of native kinetochore complexes.

Keywords centromere; centromeric nucleosome; chromosome segregation; kinetochore; TIRF microscopy

Subject Categories Cell Cycle; Chromatin, Transcription & Genomics

DOI 10.15252/emboj.2023114534 | Received 16 May 2023 | Revised 27 June 2023 | Accepted 4 July 2023 | Published online 20 July 2023

The EMBO Journal (2023) 42: e114534

Introduction

Replicated chromosomes must be accurately segregated to opposite poles during mitosis, a process that relies on their attachment to mitotic spindle microtubules via a conserved megadalton-sized protein network called the kinetochore (Santaguida & Musacchio, 2009; Biggins, 2013; Cheeseman, 2014; Musacchio & Desai, 2017; Kixmoeller *et al*, 2020). Errors in this process can lead to the rapid accumulation of mis-segregated chromosomes resulting in a cellular condition called aneuploidy, a hallmark of cancerous cells (Holland

& Cleveland, 2009; Sheltzer *et al*, 2011; Gordon *et al*, 2012; Herman *et al*, 2015). To ensure the fidelity of this process, kinetochores are assembled each cell cycle onto defined regions of chromosomes called centromeres (Clarke & Carbon, 1985; Cleveland *et al*, 2003; McAinsh & Marston, 2022). Among different organisms, centromeres vary in size and architecture and are epigenetically defined by the recruitment of a specialized H3 histone variant called CENP-A (Palmer *et al*, 1991; Sullivan *et al*, 1994). The centromere-specific targeting and deposition of CENP-A relies upon an essential conserved chaperone protein, HJURP (Camahort *et al*, 2007; Mizuguchi *et al*, 2007; Stoler *et al*, 2007; Dunleavy *et al*, 2009; Foltz *et al*, 2009). Once established, this specialized CENP-A nucleosome is then recognized by specific kinetochore proteins that enable complete kinetochore complex formation (McKinley & Cheeseman, 2016). CENP-A deposition onto centromeres is tightly regulated in cells as ectopic mis-incorporation contributes to chromosomal instability (CIN) (Shrestha *et al*, 2017). Consistent with this, CENP-A and HJURP overexpression, which can be driven by p53 loss, are common among various cancer types and have emerged as therapeutic cancer targets because higher levels are correlated with poor prognosis (Filipescu *et al*, 2017; Mahlke & Nechemia-Arbely, 2020).

Centromeric nucleosomes are critical for chromosome segregation, so it is surprising that the only widely conserved feature of centromeric DNA, its AT-rich content, is canonically a poor template for nucleosome assembly in reconstitutions with purified recombinant proteins (Kunkel & Martinson, 1981; Prunell, 1982). As a result of this, reconstitutions of assembled centromeric histones with centromeric DNA *in vitro* results in intrinsically unstable nucleosomes, making it difficult to study the functional role of the AT-rich centromeric DNA (Dechassa *et al*, 2011, 2014; Xiao *et al*, 2011). Recent breakthrough structural studies of CENP-A nucleosomes assembled with native centromeric DNA have found a more loosely associated centromeric DNA-nucleosome complex, which may provide distinct binding sites for the recruitment of DNA-binding kinetochore proteins (Zhou *et al*, 2019; Guan *et al*, 2021). However, these reconstitutions required the use of a single-chain antibody fragment (scFv) to stabilize the nucleosome in both yeast and human reconstitutions (Zhou *et al*, 2019; Guan *et al*, 2021). More complex reconstitutions that included additional kinetochore proteins required modification of the centromeric DNA sequence to include

¹ Basic Sciences Division, Howard Hughes Medical Institute, Fred Hutchinson Cancer Center, Seattle, WA, USA

² Department of Physiology and Biophysics, University of Washington, Seattle, WA, USA

³ Shared Resources, Fred Hutchinson Cancer Center, Seattle, WA, USA

*Corresponding author. Tel: +1 206 667 1351; E-mail: sbiggins@fredhutch.org

the nucleosome positioning Widom 601 DNA (Lowary & Widom, 1998; Yan *et al*, 2018; Guan *et al*, 2021; preprint: Dendooven *et al*, 2022), underscoring the difficulty of reconstituting stable kinetochore structures on centromeric DNA. While a more complete reconstitution of the constitutively centromere-associated network (CCAN) kinetochore proteins assembled onto a CENP-A nucleosome was achieved on α -satellite DNA, the functional role of AT-rich centromeric DNA remains unclear (Yatskevich *et al*, 2022).

In contrast to most eukaryotes, budding yeast have sequence-specific point centromeres consisting of similar but not identical ~ 125 bp DNA segments containing three different centromere-defining elements, CDEI, CDEII, and CDEIII (Carbon, 1984; Carbon & Clarke, 1984; Biggins, 2013). CDEI and CDEIII have consensus sites to recruit the centromere binding factors 1 and 3 (Cbf1 and CBF3), respectively. One function of Cbf1 is to protect centromeres from transcription to ensure chromosome stability (Cai & Davis, 1990; Hedouin *et al*, 2022), while the CBF3 complex (consisting of Ctf3, Cep3, Skp1, and Ndc10) coordinates with the Cse4 (CENP-A in humans) specific chaperone Scm3 (HJURP in humans) to promote the deposition of Cse4^{CENP-A} at CDEII (Camahort *et al*, 2007; Cole *et al*, 2011; Cho & Harrison, 2011b; Guan *et al*, 2021). Similar to other organisms, the CDEII element lacks sequence homology but consists of highly AT-rich DNA (Guan *et al*, 2021). Changes in the length or AT-content of CDEII compromise centromere stability *in vivo* for unknown reasons (Clarke & Carbon, 1985; Cumberledge & Carbon, 1987; Gaudet & Fitzgerald-Hayes, 1987). More recently, the presence of homopolymeric runs of A and T within the CDEII elements were identified to play a significant role in centromere function *in vivo* (Baker & Rogers, 2005), but the underlying mechanism requiring these homopolymeric runs remains unknown due to the inherent instability of these nucleosomes *in vitro* (Dechassa *et al*, 2011, 2014; Xiao *et al*, 2011). One possibility is that these sequences play a role in exclusion of the canonical H3 nucleosome, as H3 eviction has been proposed as a potential function of centromeres (Dechassa *et al*, 2011; Shukla *et al*, 2018). Due to their difficulty to study in cells, it remains unclear why these CDEII centromere sequences are essential *in vivo* yet are such poor templates for nucleosome formation and kinetochore assembly *in vitro*.

To resolve this paradox between the requirements for centromere sequence in nucleosome formation *in vitro* versus *in vivo*, it is imperative to determine what additional factors stabilize centromeric nucleosomes in a physiological context. Recent structural reconstitutions that contain a Cse4^{CENP-A} nucleosome in complex with additional inner kinetochore proteins (CCAN) have identified significant interactions between centromeric DNA and inner kinetochore proteins around the nucleosome (Yan *et al*, 2019; Guan *et al*, 2021). These reconstitutions have provided insight into potential candidate factors, yet the use of non-native centromeric DNA limits model testing. Unfortunately, studying the formation of centromeric nucleosomes in cells is extremely challenging because the centromeres are too close to be resolved individually by light microscopy and because they remain fully occupied for most of the cell cycle (Joglekar *et al*, 2006; Dhatchinamoorthy *et al*, 2017).

To address these limitations, we developed a new technique utilizing total internal reflection fluorescent microscopy (TIRFM) to enable direct observation of centromeric nucleosome formation with single molecule resolution. Our approach was inspired by the “colocalization single molecule spectroscopy” (CoSMoS) studies of DNA

transcription and RNA splicing complexes (Friedman *et al*, 2006; Hoskins *et al*, 2011; Friedman & Gelles, 2012). In our adaptation of the technique, individual centromere DNAs are linked sparsely to a glass surface and formation of single Cse4^{CENP-A} nucleosomes on the individual DNAs is observed in cell extract in real time. To achieve this resolution, *Saccharomyces cerevisiae* was used as a model system due to their simplified and sequence-defined point centromeres that contain only a single Cse4^{CENP-A} nucleosome (Furuyama & Biggins, 2007; Cole *et al*, 2011). Stable recruitment of Cse4^{CENP-A} was highly specific and dependent upon native centromere sequence, recapitulating *in vivo* requirements for nucleosome formation. Through continuous visualization of individual centromeres, we observed unexpectedly dynamic association of Cse4^{CENP-A}. Specifically, we found that Cse4^{CENP-A} deposition occurred in two distinct steps: first, a “targeting” step, consisting of a reversible binding of Cse4^{CENP-A} for which Scm3^{HJURP} was dispensable, followed by a second “stabilization” step, for which Scm3^{HJURP} and DNA-binding CCAN kinetochore proteins were required. Stabilization was blocked by constraining both ends of the centromeric DNA template, suggesting that it also requires DNA wrapping around the Cse4^{CENP-A} nucleosome. Stabilization was also significantly influenced by both the sequence composition of the CDEII element and the subsequent binding of inner kinetochore proteins during kinetochore assembly. Together, these findings shed new light on the mechanisms that catalyze formation of a robust centromeric DNA-based platform for kinetochore assembly and provide a foundation to address additional steps in the kinetochore assembly process.

Results

Efficient recruitment of Cse4^{CENP-A} to individual centromeric DNAs

To study the requirements and dynamics of centromeric nucleosome assembly, we adapted our recently developed method for bulk assembly of yeast kinetochores *de novo* in cell extracts (Lang *et al*, 2018), modifying it for single molecule imaging via TIRFM. Template DNAs consisting of the chromosome III centromere (117 bp), with ~ 70 bp of pericentromeric DNA plus ~ 250 bp of linker DNA on each side (referred to as “CEN DNA”), were linked sparsely to a streptavidin-functionalized coverslip surface through biotin tags (Crawford *et al*, 2008) (Fig 1A). Dye-labels added to the free ends of the DNAs allowed their visualization at the single molecule level. Introducing whole cell extracts prepared from strains with fluorescent kinetochore proteins into the chamber enabled the recruitment and retention of the labeled kinetochore proteins on $\sim 1,000$ individual CEN DNA molecules to be monitored in a single field of view. Initially, we performed simple endpoint analyses, where we incubated cell lysate for 90 min with surface-linked CEN DNAs, washed the lysate from the chamber and then measured colocalization from individual images.

We first tested whether Cse4^{CENP-A} and the CBF3 complex, which is required for Cse4^{CENP-A} localization *in vivo*, were specifically recruited to the individual CEN DNA molecules (Cho & Harrison, 2011a; Lang *et al*, 2018). Using extracts from cells expressing endogenously tagged Ndc10-mCherry, a CBF3 complex component (Fig 1B), we observed high endpoint colocalization of Ndc10

on CEN DNA (~ 70%, Fig 1C-left panel). To ensure specific colocalization, we tested a mutant CEN DNA template (CDEIII^{mut}) with two substitutions that prevent CBF3 complex binding

(McGrew et al, 1986; Lang et al, 2018). Ndc10-mCherry endpoint colocalization on this mutant template was nearly abolished (Fig 1C-right panel). We next sought to monitor endpoint colocalization of

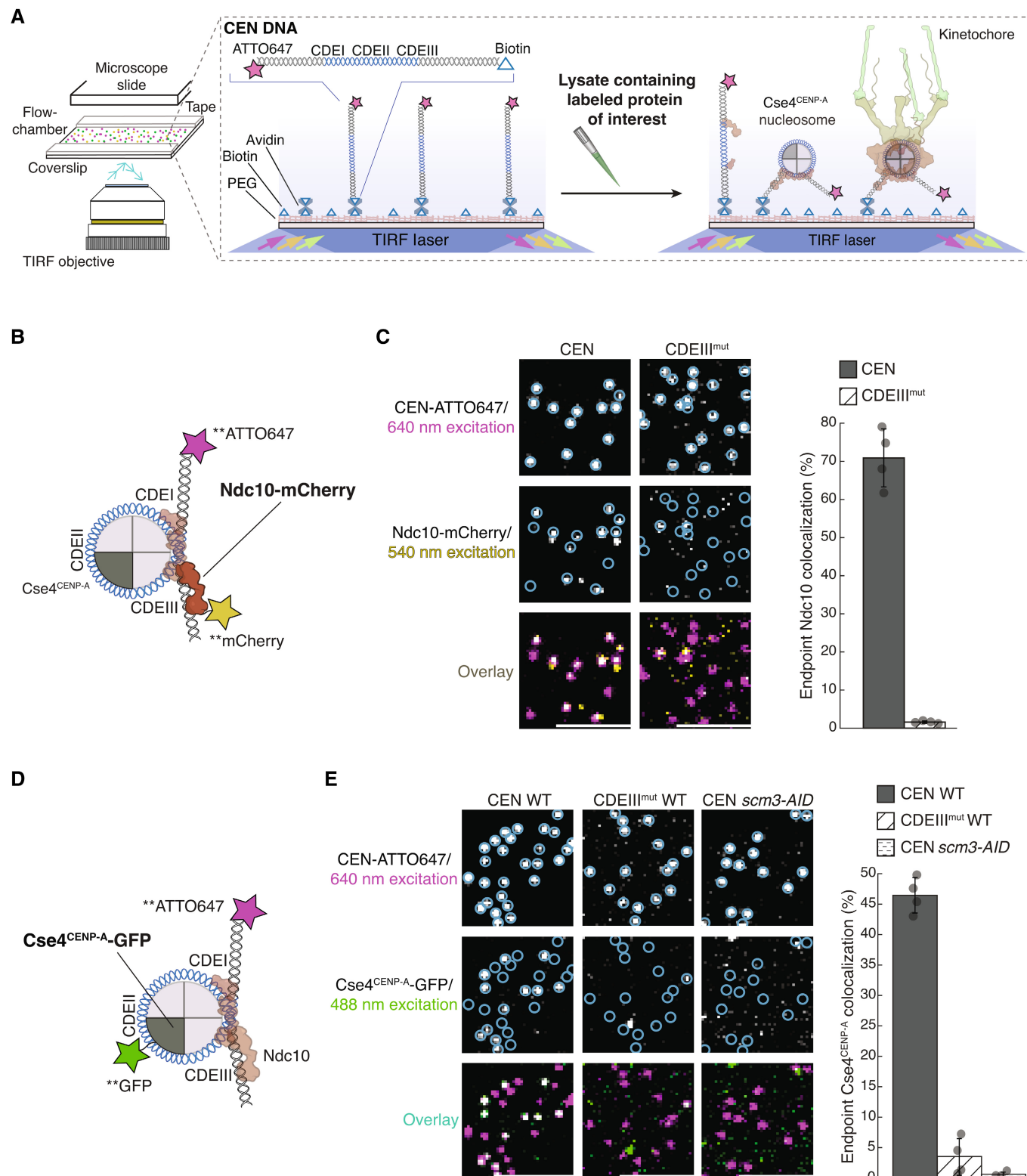


Figure 1.

Figure 1. Ndc10 and Cse4^{CENP-A} assemble with high efficiency and specificity onto CEN DNAs in extract.

- A Schematic of the TIRFM colocalization assay. Yeast lysate containing a fluorescent protein(s) of interest is added to a coverslip with immobilized fluorescent CEN DNA. After incubation, the lysate is washed from the chamber and the CEN DNA and fluorescent kinetochore proteins are imaged via TIRFM.
- B Schematic of fluorescent label location around the centromeric nucleosome used in (C) for colocalization imaging.
- C Example images of TIRFM endpoint colocalization assays. Top panels show CEN DNA (Top-left panel, blue circles) or CDEIII^{MUT} CEN DNA (top-right panel, blue circles) visualized in lysates containing Ndc10-mCherry. Middle panels show the visualized Ndc10-mCherry on CEN DNA (middle-left panel) or CDEIII^{MUT} DNA (middle-right panel) with colocalization shown in relation to blue DNA circles. Bottom panels show overlay of DNA channel (magenta) with Ndc10-mCherry (yellow) on CEN DNA (bottom-left panel) or CDEIII^{MUT} DNA (bottom-right panel). Scale bars 3 μ m. Graph shows the quantification of Ndc10 endpoint colocalization on CEN DNA and on CDEIII^{MUT} CEN DNA ($70 \pm 7.6\%$, $1.6 \pm 0.3\%$ respectively, avg \pm s.d. $n = 4$ experiments, each examining $\sim 1,000$ DNA molecules from different extracts).
- D Schematic of fluorescent label location around the centromeric nucleosome used in (E) for colocalization imaging.
- E Example images of TIRFM endpoint colocalization imaging. Top panels show CEN DNA (top-left panel, blue circles) or CDEIII^{MUT} CEN DNA (top-middle panel, blue circles) visualized in lysates that included Cse4^{CENP-A}-GFP or CEN DNA in lysates that lacked Scm3^{HJURP} (*scm3-AID*) (top-right panel, blue circles). Middle panels show Cse4^{CENP-A}-GFP visualized on CEN DNA (middle-left panel) or CDEIII^{MUT} CEN DNA (center panel) or on CEN DNA in lysates lacking Scm3^{HJURP} (*scm3-AID*) (middle-right panel) with colocalization shown in relation to blue DNA circles. Bottom panels show overlay of CEN DNA channel (magenta) with Cse4^{CENP-A}-GFP (green) on CEN DNA (bottom-left panel) or CDEIII^{MUT} DNA (bottom-middle panel) or on CEN DNA in lysates lacking Scm3^{HJURP} (*scm3-AID*) (bottom-right panel). Scale bars 3 μ m. Graph shows quantification of observed colocalization of Cse4 on CEN DNA and on CDEIII^{MUT} CEN DNA or on CEN DNA in lysates that lacked Scm3^{HJURP} ($47 \pm 2.9\%$, $3.5 \pm 3.0\%$ and $0.6 \pm 0.4\%$ respectively, avg \pm s.d. $n = 4$ experiments, each examining $\sim 1,000$ DNA molecules from different extracts).

Cse4^{CENP-A}-GFP using an internal Cse4 tag that is fully functional (Fig 1D), as it was previously shown that the position of the GFP tag in Cse4 affects protein function (Wisniewski *et al*, 2014). Cse4^{CENP-A}-GFP showed high endpoint colocalization of $\sim 50\%$ (Fig 1E-left panel). This localization was specific because it was nearly abolished on the CDEIII^{mut} DNA template (Fig 1E-middle panel), consistent with the CBF3 complex being required for Cse4^{CENP-A} centromere localization (Cho & Harrison, 2011a; Lang *et al*, 2018). Likewise, proteasomal degradation of the essential chaperone Scm3^{HJURP} also prevented Cse4^{CENP-A} from colocalizing to CEN DNAs (Nishimura *et al*, 2009; Lang *et al*, 2018) (Fig 1E-right panel). To further probe the fidelity of the assay, we quantified the stoichiometry of Ndc10 and Cse4^{CENP-A} via photobleaching assays. The Ndc10-mCherry that colocalized with CEN DNA photobleached predominantly in two steps (Appendix Fig S1A and B) with a step distribution similar to other previously characterized dimeric proteins (Popchok *et al*, 2017, 2018). This is consistent with structural studies showing that Ndc10 is a homodimer within the CBF3 complex and with the range of stoichiometries reported *in vivo* (Joglekar *et al*, 2006; Cho & Harrison, 2011a; Wisniewski *et al*, 2014; Leber *et al*, 2018; Guan *et al*, 2021). The Cse4^{CENP-A} that colocalized with CEN DNA yielded similar results, with the majority of Cse4^{CENP-A}-GFP photobleaching in two steps (Appendix Fig S1C and D), as expected based on nucleosome reconstitutions and consistent with fluorescence and photobleaching analyses of Cse4^{CENP-A} at centromeres *in vivo* (Joglekar *et al*, 2006; Camahort *et al*, 2007; Aravamudan *et al*, 2013; Guan *et al*, 2021). Taken together, these results show that recruitment of Cse4^{CENP-A} onto individual CEN DNAs depends on the known requirements *in vivo* and suggest that the copy numbers of both Ndc10 and Cse4^{CENP-A} recruited onto the DNAs match their copy numbers at kinetochores *in vivo*.

Cse4^{CENP-A} binds more stably when preceded by CBF3 complex component Ndc10

We next set out to monitor the dynamics of Ndc10 and Cse4^{CENP-A} centromere targeting by performing continuous time-lapse TIRFM. We tagged Ndc10 with mCherry in cells also expressing GFP-labeled Cse4^{CENP-A} to allow simultaneous detection in separate color channels (Fig 2A). To assist in the analysis of colocalization events taking place on hundreds of CEN DNA templates simultaneously, we developed an automated analysis software package in MATLAB (see

Materials and Methods). Briefly, we collected a 45-min TIRFM time-lapse with acquisitions every 5 s in the protein channels (488 and 568 nm) and every 60 s in the DNA channel (647 nm). The software identified CEN DNAs and then subsequently monitored both protein channels to determine colocalization residence lifetimes at each CEN DNA (Fig 2A), enabling the rapid quantification of many independent colocalization events within a single field of view. We applied this analysis to simultaneously measure residence lifetimes for both Ndc10 and Cse4^{CENP-A} (Figs 2A and EV1A). Kaplan–Meier analysis of the estimated survival functions showed that Cse4^{CENP-A} had a shorter median lifetime (approximately half) than the median Ndc10 lifetime (Fig 2B). We note that occasionally one of the proteins was present when imaging began or persisted until the acquisition ended (censored events). To avoid the potential exclusion of long-lived residences and because these censored events were typically $< 5\%$ of the total residences observed, they were included in this analysis. To ensure that the dynamic Cse4^{CENP-A} behavior we observed was not a consequence of a particular CEN sequence, we performed residence lifetime assays on several CEN templates from different chromosomes. The median Cse4^{CENP-A} lifetimes were similar between varying chromosome CEN templates (103, 103, and 109 s), all shorter than the median survival time of Ndc10 (Appendix Fig S2A). Consistent with this, we also confirmed similar Cse4^{CENP-A} endpoint colocalization recruitment on several different CEN templates (Appendix Fig S2B and C). During this analysis, we found that the Cse4^{CENP-A}-CEN DNA endpoint colocalization was lower in genetic backgrounds where Cse4^{CENP-A} and another kinetochore protein were fluorescently tagged compared to when only Cse4^{CENP-A} was tagged, likely due to mild genetic interactions between tagged proteins. However, this did not prevent analyses of the arrival times and residence lifetimes of the tagged components relative to one another.

The dynamic behavior of Cse4^{CENP-A} was surprising since it has been reported to be stably bound to centromeres *in vivo* outside of S phase (Joglekar *et al*, 2008; Wisniewski *et al*, 2014). However, the transient Cse4^{CENP-A}-CEN DNA interactions that we readily detected in our single molecule assays would be undetectable *in vivo* due to reduced signal-to-noise and poorer time resolution. We considered two factors that could contribute to the dynamic Cse4^{CENP-A} behavior we observed. First, the cellular extracts could contain negative regulatory factors, such as chromatin remodelers that counter nucleosome formation. To test this, we removed the lysate and analyzed

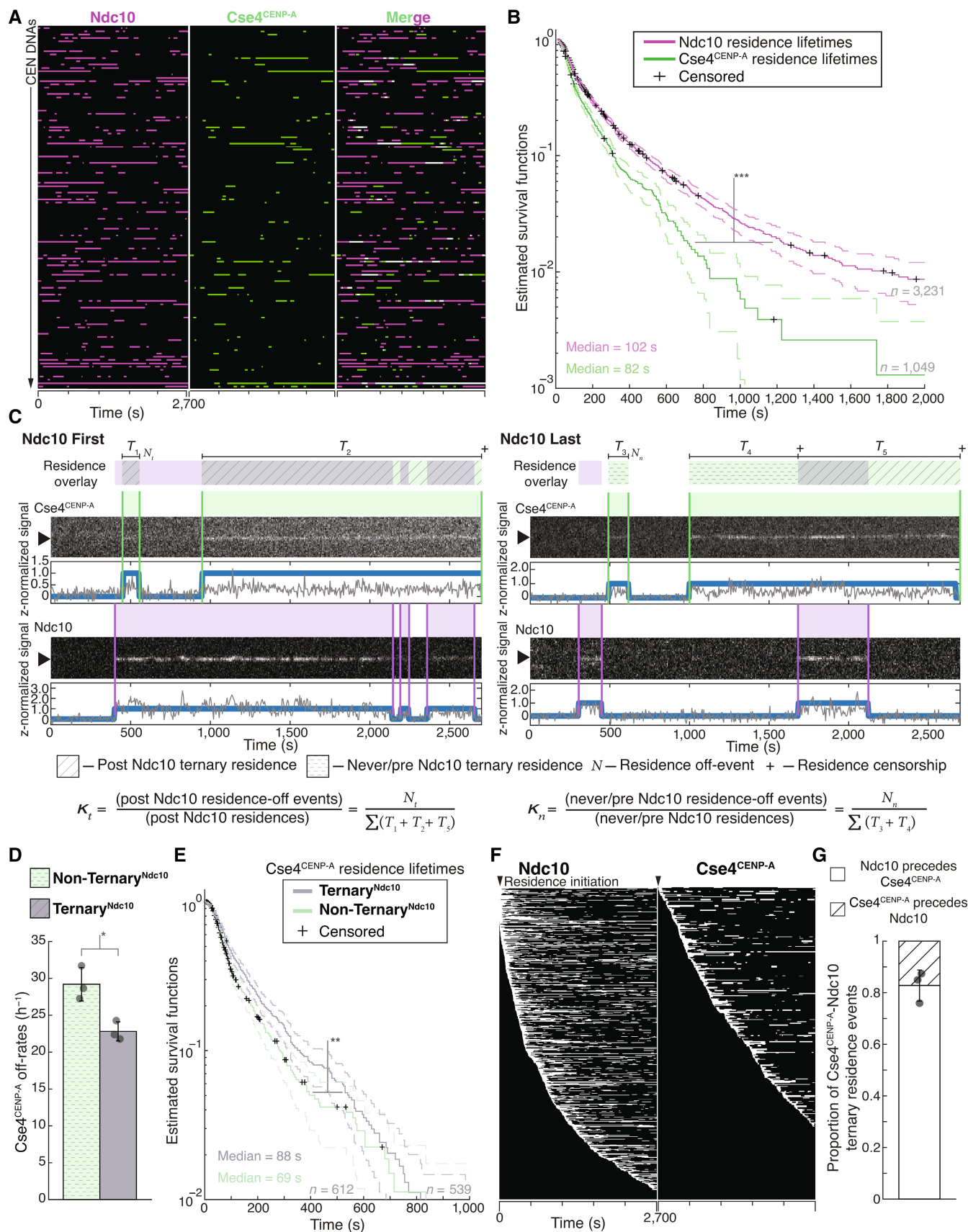


Figure 2.

Figure 2. Ndc10 stabilizes Cse4^{CENP-A} on CEN DNA.

- A Example graph of total identified colocalization residences observed on CEN DNA per imaging sequence. Each row represents one identified CEN DNA with all identified residences shown over entire imaging sequence (2,700 s) for Ndc10 (magenta) and Cse4^{CENP-A} (green). Instances where Ndc10 and Cse4^{CENP-A} residence coincides (white-merge) represent simultaneous observation of both proteins on single CEN DNA, termed ternary residences. Complete series shown in Fig EV1A.
- B Estimated survival function plots of Kaplan–Meier analysis of CEN DNA residence lifetimes of Ndc10 (magenta—median lifetime of 102 s, $n = 3,231$ over three experiments of $\sim 1,000$ DNA molecules using different extracts) and Cse4^{CENP-A} (red—median lifetime of 79 s, $n = 1,049$ over three experiments of $\sim 1,000$ DNA molecules using different extracts). Significant difference between ternary Ndc10 residence lifetime survival plots (***) compared to Cse4^{CENP-A} (two-tailed P -value of 0 as determined by log-rank test). 95% confidence intervals indicated (dashed lines), right-censored lifetimes (plus icons) were included and unweighted in survival function estimates.
- C Schematic for off-rate estimate calculations with representative residence lifetime assay traces of Ndc10 and Cse4^{CENP-A} on CEN DNA. Example kymographs of Cse4^{CENP-A} (top—488 nm) and Ndc10 (bottom—568 nm) in relation to a single identified CEN DNA (arrow), with normalized intensity trace below (gray) as well as identified colocalization residences (blue). Ndc10 First example (left) illustrates Ndc10 colocalization that precedes Cse4^{CENP-A}, yielding only Ternary^{Ndc10} Cse4^{CENP-A} residences. Ndc10 Last example (right) illustrates Cse4^{CENP-A} colocalization that precedes Ndc10, yielding both Non-Ternary^{Ndc10} Cse4^{CENP-A} residences and Ternary^{Ndc10} Cse4^{CENP-A} residence after Ndc10 colocalization initiation. Images were acquired every 5 s with normalized fluorescence intensity shown in arbitrary units. Bottom panel includes formulas used to calculate the ternary Cse4^{CENP-A} off-rate, k_t , where N_t represents the total number of apparent Cse4-GFP detachments recorded during ternary residences, and $\sum(T_1 + T_2 + T_5)$ represents the total amount of ternary residence time observed. In addition, the formula for non-ternary Cse4 off-rate, k_n , where N_n represents the total number of apparent Cse4-GFP detachments recorded during non-ternary residences, and $\sum(T_3 + T_4)$ represents the total amount of non-ternary residence time observed.
- D Cse4^{CENP-A} has slower off-rates after colocalization with Ndc10 on CEN DNA. Quantification of the estimated Cse4^{CENP-A} off-rates of the Non-Ternary^{Ndc10} and Ternary^{Ndc10} pools ($29 \pm 2 \text{ h}^{-1}$ and $22 \pm 1 \text{ h}^{-1}$ respectively, avg \pm s.d. $n = 1,151$ over three experiments of $\sim 1,000$ DNA molecules using different extracts). Significant difference between off-rates (*) with a P -value of 0.02 as determined by two-tailed unpaired t -test.
- E Kaplan–Meier analysis of Ternary^{Ndc10} residence lifetimes of Cse4^{CENP-A} on CEN DNA (purple—median lifetime of 88 s, $n = 539$ over three experiments of $\sim 1,000$ DNA molecules using different extracts) and of Non-Ternary^{Ndc10} Cse4^{CENP-A} residence lifetimes (teal—median lifetime of 69 s, $n = 612$ over three experiments of $\sim 1,000$ DNA molecules using different extracts). There is a significant difference (**) between Ternary^{Ndc10} and Non-Ternary^{Ndc10} lifetime survival plots (two-tailed P -value of $7.4\text{e-}4$ as determined by log-rank test). 95% confidence intervals indicated (dashed lines), right-censored lifetimes (plus icons) were included and unweighted in survival function estimates.
- F Example plot of total identified residences observed on CEN DNA per imaging sequence of Ndc10 (left) and Cse4^{CENP-A} (right) independently sorted by residence initiation time, starting at the top with initiation time of 0 s (arrow).
- G Timing of all non-simultaneous Ndc10 and Cse4^{CENP-A} ternary residence events. The proportion when Ndc10 precedes Cse4^{CENP-A} is 0.83 ± 0.06 and when Cse4^{CENP-A} precedes Ndc10 is 0.17 ± 0.06 (avg \pm s.d., $n = 504$ over three experiments of $\sim 1,000$ DNA molecules using different extracts). Simultaneous arrival defined as residence initiation within 5 s of each other and comprise 0.07 ± 0.04 of all ternary residence events (avg \pm s.d., $n = 35$ over three experiments of $\sim 1,000$ DNA molecules using different extracts).

protein stability on the CEN DNA. Remarkably, Cse4^{CENP-A} and Ndc10 exhibited $\sim 70\%$ retention on CEN DNA after 24 h incubation in buffer at 25°C (Fig EV1B and C), suggesting there are factors in the lysate that actively disrupt the centromeric nucleosome. Second, we considered the possibility that photobleaching could make Cse4^{CENP-A} appear dynamic. To address this, we estimated the photo-stability of the fluorophores by measuring their respective lifetimes under our imaging parameters and found that the Ndc10 residence lifetimes (Fig EV1D) were more potentially limited by photo-stability than the Cse4^{CENP-A} lifetimes (Fig EV1E), the majority of which were not truncated by photobleaching. Despite photobleaching limiting some residence lifetimes, the relationships we observed in residence lifetime assays were consistent with trends observed in the endpoint colocalization assays. For example, the longer median lifetime of Ndc10 compared to Cse4^{CENP-A} (102 vs. 79 s) correlated with higher endpoint colocalization (70 vs. 47%). Taken together, these data suggest that Cse4^{CENP-A} is initially more dynamic than Ndc10 at centromeres, prior to its stable incorporation.

To further dissect the lifetime differences between Ndc10 and Cse4^{CENP-A}, we sought to determine if the presence of Ndc10 affected the behavior of Cse4^{CENP-A} on CEN DNA. To do this, we identified instances where a Cse4^{CENP-A} residence coincided with Ndc10 at any time on the same CEN DNA, termed “ternary residence.” To assess whether the formation of a ternary^{Ndc10} residence altered Cse4^{CENP-A} stability on CEN DNA, we sought to estimate the off-rates of Cse4^{CENP-A} in the ternary versus non-ternary contexts. Although 84% of the total Cse4^{CENP-A} ternary residence time had Ndc10 associated, we wanted to rigorously ensure there was no

selection bias for long-lived Cse4^{CENP-A} residences because they are more likely to form ternary associations. We therefore further divided the ternary^{Ndc10} Cse4^{CENP-A} residences according to the timing of Ndc10 association. When Ndc10 arrived prior to or simultaneously with Cse4^{CENP-A}, we included the entire residence time (Ndc10 First— T_1 , T_2 , Fig 2C, Movie EV1). In the cases where Cse4^{CENP-A} association preceded Ndc10, we only included the residence time after Ndc10 arrived (Ndc10 Last— T_5 , Fig 2C, Movie EV2). Because we could not differentiate between Ndc10 turnover and photobleaching, we included the entirety of a continuous Cse4^{CENP-A} residence pulse after initial ternary association with Ndc10, regardless of Ndc10 residence length or subsequent associations. For the non-ternary^{Ndc10} residences (T_3 , T_4 , Fig 2C), we included any Cse4 residence prior to the arrival of Ndc10 as well as Cse4^{CENP-A} residences where Ndc10 was never present.

To estimate off-rates for ternary and non-ternary Cse4^{CENP-A}, we counted the numbers of off-events observed in each category, N_t and N_n respectively, and divided each by the total observed times from each residence pool, $T_t = \text{SUM}(\text{of all } T_1, T_2, \text{ and } T_5)$ to calculate the off-rate k_t (Fig 2C) and $T_n = \text{SUM}(\text{of all } T_3 \text{ and } T_4)$ to calculate the off-rate k_n (Fig 2C). The off-rate for ternary^{Ndc10} Cse4^{CENP-A} was significantly lower than for non-ternary^{Ndc10}, 22/h versus 29/h, indicative of stabilization of Cse4^{CENP-A} on CEN DNA after ternary Ndc10 association (Fig 2D). We also performed Kaplan–Meier analysis to estimate their survival lifetimes and found a significant increase in the median lifetime of ternary^{Ndc10} compared to non-ternary^{Ndc10} residences (88 vs. 69 s, Fig 2E). Consistent with this stabilization, the proportion of Cse4^{CENP-A} residences that were long lived (> 300 s) after ternary^{Ndc10} association

increased approximately two-fold (Fig EV1F). While we did not estimate on-rates, comparison of Ndc10 and Cse4^{CENP-A} residence pulses when organized by their initiation times showed more rapid association of Ndc10 to CEN DNA (Fig 2F). This potential for differing on-rates may explain why when ternary associations were formed, Ndc10 typically preceded Cse4^{CENP-A} arrival to the CEN DNA (Fig 2G). We note that it was surprising to see Cse4^{CENP-A} at the CEN DNA in the absence of Ndc10. To determine whether Ndc10 is present but undetectable in these instances, we analyzed Cse4^{CENP-A} lifetimes on the mutant CDEIII^{mut} CEN DNA template which abolishes Ndc10 association. Although overall Cse4^{CENP-A} associations were reduced, we observed transient Cse4^{CENP-A} associations with significantly reduced residence lifetimes on CDEIII^{mut} CEN DNA, suggesting that Cse4 has some intrinsic CEN DNA binding in the absence of CBF3 (Fig EV1G and H). Taken together, these observations are consistent with *in vivo* findings, where it has been established that Ndc10 is required for Scm3^{HJURP}-dependent Cse4^{CENP-A} deposition, and where Ndc10 is thought to coordinate with the Cbf1 complex to promote nucleosome formation (Cho & Harrison, 2011a).

The chaperone Scm3^{HJURP} is a limiting cofactor that promotes stable Cse4^{CENP-A} association

The biphasic Cse4^{CENP-A} localization behavior, with many short colocalizations (< 120 s) and fewer long colocalizations (> 300 s), was not fully correlated with Ndc10 occupancy, as 60% of ternary^{Ndc10} Cse4^{CENP-A} residences were still short-lived. We therefore further investigated this behavior by simultaneously visualizing Cse4^{CENP-A} and its essential chaperone protein Scm3^{HJURP}, which exhibits DNA-binding activity and is required for Cse4^{CENP-A} centromere localization in cells (Camahort et al, 2007; Mizuguchi et al, 2007; Stoler et al, 2007; Xiao et al, 2011) (Fig 3A, Movie EV3). Residence lifetimes for Scm3^{HJURP} on CEN DNA were shorter than Cse4^{CENP-A} lifetimes (Figs 3A and B, and EV2A and B), consistent with its faster turnover rate *in vivo* (Wisniewski et al, 2014). To estimate the fraction of time Scm3^{HJURP} and Cse4^{CENP-A} colocalized together on CEN DNA, we analyzed the ternary^{Scm3} residence times. We found that Scm3^{HJURP} co-occupied the CEN DNA an average of 56.0% ($n = 393$) of the total Cse4^{CENP-A} residence time, a lower occupancy rate than that of Ndc10 and Cse4^{CENP-A} (84.3%), as expected given its more rapid turnover. Strikingly, we discovered a high proportion of total Cse4^{CENP-A} residences that occurred without Scm3^{HJURP} (0.78 vs. 0.22, Fig 3C), which was unexpected because Scm3^{HJURP} is thought to be required to target Cse4^{CENP-A} to centromeres *in vivo* (Camahort et al, 2007; Stoler et al, 2007).

We next assayed whether the two distinct Cse4^{CENP-A} residence subpopulations, ternary^{Scm3} and non-ternary^{Scm3}, behaved differently by quantifying their estimated off-rates as described for Ndc10 (Fig 2C). We found a significant decrease in the average off-rate of ternary^{Scm3} Cse4^{CENP-A} residences when compared to non-ternary^{Scm3} (26 vs. 21 h⁻¹, Fig 3D). Consistent with this observed stabilization of Cse4^{CENP-A} after Scm3^{HJURP} association and the requirement for Scm3^{HJURP} to localize Cse4^{CENP-A} to centromeres *in vivo*, the proportion of Cse4^{CENP-A} residences that were long lived (> 300 s) increased approximately two-fold among the ternary^{Scm3} events (Fig 3E). We also performed Kaplan–Meier analysis to estimate their survival lifetimes and found a significant increase in the

median lifetime of ternary^{Scm3} residences when compared to non-ternary^{Scm3} (108 vs. 79 s, Fig 3F). Together, these results are consistent with Scm3^{HJURP} stabilizing Cse4^{CENP-A} at centromeres and then rapidly exchanging after Cse4^{CENP-A} incorporation (Wisniewski et al, 2014).

To further dissect the role of Scm3^{HJURP} in Cse4^{CENP-A} centromere localization, we calculated the off-rates for Scm3^{HJURP} in ternary^{Cse4} and non-ternary^{Cse4} contexts. Unlike Cse4^{CENP-A}, Scm3^{HJURP} was not significantly stabilized after ternary association with Cse4^{CENP-A}, as the off-rates and median lifetimes of both contexts were similar (Fig EV2C and D). These findings are consistent with a model of Scm3^{HJURP} turnover after association with Cse4^{CENP-A}. Next, we assayed the relative arrival order of Cse4^{CENP-A} versus Scm3^{HJURP} on CEN DNA. Contrary to models that suggest the chaperone delivers Cse4^{CENP-A} to centromeres, only ~20% of the ternary^{Scm3} residences resulted from co-arrival of Cse4^{CENP-A} and Scm3^{HJURP} (Fig EV2E). The remaining ternary associations consisted of 46% where Scm3^{HJURP} preceded Cse4^{CENP-A} and 34% where Cse4^{CENP-A} preceded Scm3^{HJURP} (Fig EV2E). Residence lifetimes of these differing ternary pools were similar, with no significant difference in estimated survival plots (Fig EV2F). This is consistent with our findings that Cse4^{CENP-A} can interact with the centromere in the absence of Scm3^{HJURP} (Fig 3C) and suggests that Scm3^{HJURP} catalyzes stable Cse4^{CENP-A} incorporation at centromeric DNA instead of delivering it to the centromere. Cse4^{CENP-A} centromere targeting is thought to occur through Scm3^{HJURP} binding to Ndc10, so we next monitored their behavior on mutant CDEIII^{mut} CEN DNA that lacks Ndc10 in lifetime residence assays (Fig EV3A). Strikingly, Scm3^{HJURP} residences were significantly increased when compared to those on CEN DNA (Fig EV3B), suggesting its intrinsic DNA-binding activity may be the primary driver of its CEN DNA binding and that stable Cse4^{CENP-A} association is required for its turnover (Xiao et al, 2011). In contrast, Cse4^{CENP-A} residences on CDEIII^{mut} CEN DNA had a much shorter median survival time compared to its CEN counterpart (Fig EV2C), consistent with Ndc10 and Scm3^{HJURP} stabilizing its association. In addition, the stabilization of Cse4^{CENP-A} after Scm3^{HJURP} association that was observed on CEN DNA (Fig 3D) was lost, as the lifetimes of ternary^{Scm3} and non-ternary^{Scm3} residences on CDEIII^{mut} CEN were similar (Fig EV3C). Taken together, these data are consistent with a requirement for Ndc10 in the localization of Cse4^{CENP-A} but not necessarily through Scm3 recruitment. One possibility is there is cooperativity between Ndc10 and Scm3^{HJURP} and both DNA-binding proteins must be present simultaneously at CEN DNA to promote stable Cse4^{CENP-A} incorporation.

Our finding that there was a population of Cse4^{CENP-A} lacking its chaperone led us to test whether the chaperone is limiting for stable Cse4^{CENP-A} centromere localization. To do this, we modified the availability of the Cse4^{CENP-A}/Scm3^{HJURP} complex *in vivo* to assess resulting changes in Cse4^{CENP-A} behavior. The E3 ubiquitin ligase Psh1 and the chaperone Scm3^{HJURP} directly compete for Cse4^{CENP-A} binding (Zhou et al, 2021). We therefore reasoned that the amount of Cse4^{CENP-A}-Scm3^{HJURP} complex in cells should be reduced by overexpressing Psh1 and, conversely, that the amount of Cse4^{CENP-A}-Scm3^{HJURP} complex might be increased by overexpressing Scm3^{HJURP}. To test these predictions, we introduced an ectopic copy of either Psh1 or Scm3^{HJURP} under an inducible GAL promoter into cells containing labeled Cse4^{CENP-A} and Scm3^{HJURP}. Inducing short pulses of either protein did not significantly alter the total

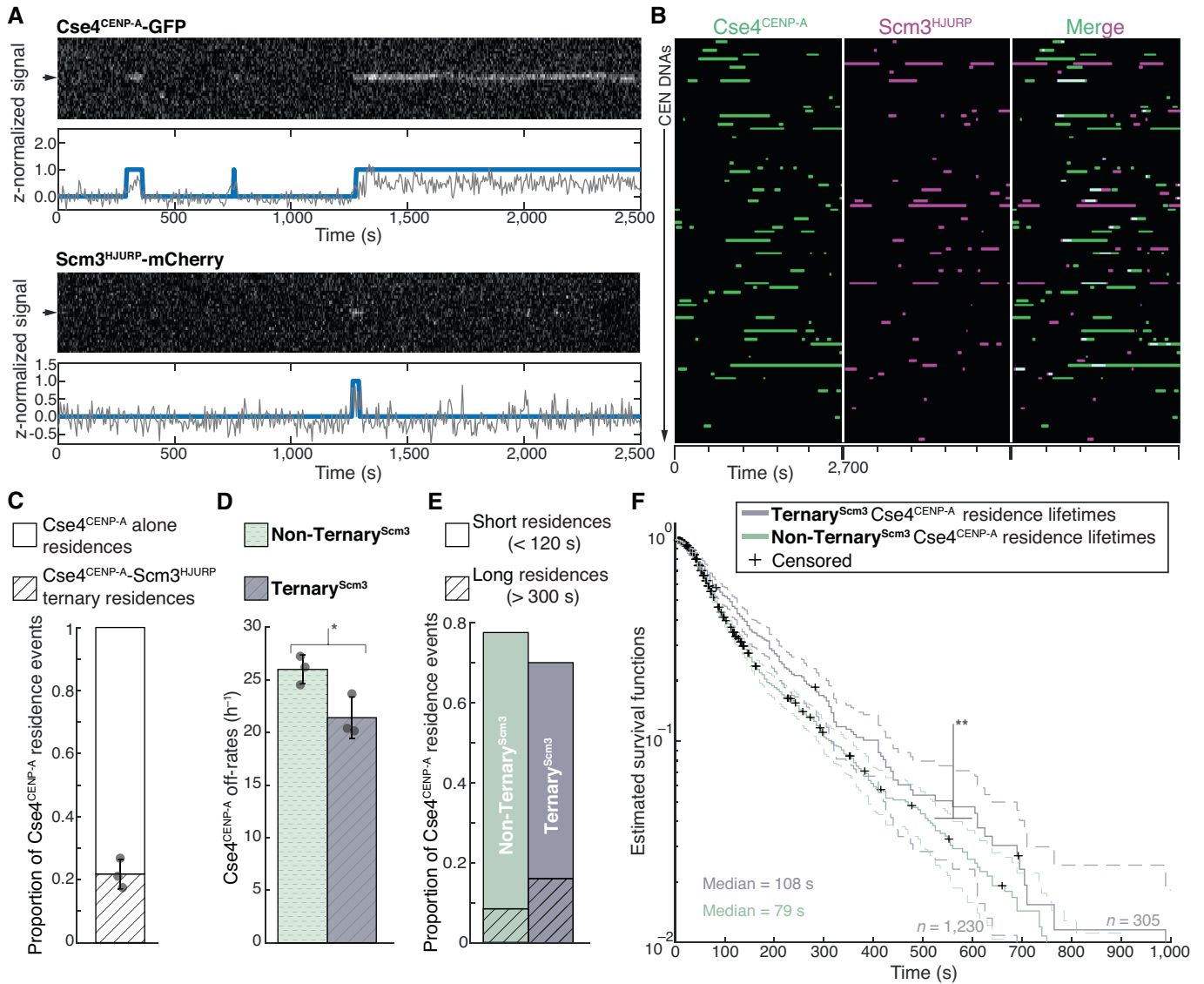


Figure 3. Cse4^{CENP-A} residence time on centromeric DNA is increased in the presence of its chaperone Scm3^{HJURP}.

A Representative residence lifetime assay traces of Cse4^{CENP-A} and Scm3^{HJURP} on a single CEN DNA. Top panel includes kymograph of Cse4^{CENP-A} (top-488 nm) in relation to single identified CEN DNA (arrow), with normalized intensity trace (gray-bottom) as well as identified residences (blue). Bottom panel includes kymograph of Cse4^{CENP-A} (bottom-568 nm) in relation to the same identified CEN DNA (arrow), with normalized intensity trace (gray-bottom) as well as identified residences (blue). Images acquired every 5 s with normalized fluorescence intensity shown in arbitrary units.

B Example plot of total identified residences observed on CEN DNA per imaging sequence. Each row represents one identified CEN DNA with all identified residences shown over entire imaging sequence (2,700 s) for Cse4^{CENP-A} (green) and Scm3^{HJURP} (magenta). Cases where Scm3^{HJURP} and Cse4^{CENP-A} residence coincides represent simultaneous observation of both proteins on single CEN DNA, termed ternary residence (merge, white). Complete plot shown in Fig EV2A.

C Quantification of the proportion of Cse4^{CENP-A} and Scm3^{HJURP} ternary residences with CEN DNA compared to CEN DNA residences of Cse4^{CENP-A} alone (0.22 ± 0.05 and 0.78 ± 0.05 respectively, avg ± s.d. n = 1,419 over three experiments of ~1,000 DNA molecules using different extracts). Ternary residences include simultaneous Scm3^{HJURP} residence at any point during continuous Cse4^{CENP-A} residence on CEN DNA.

D Quantification of the estimated off-rates of Cse4^{CENP-A} that never formed a ternary residence (Non-Ternary^{Scm3}) and of Cse4^{CENP-A} after ternary residence with Scm3^{HJURP} (Ternary^{Scm3}) on CEN DNA (26 h⁻¹ ± 1 h⁻¹ and 21 h⁻¹ ± 2 h⁻¹ respectively, avg ± s.d. n = 1,535 over three experiments of ~1,000 DNA molecules using different extracts). Significant difference between off-rates (*) with a P-value of 0.03 as determined by two-tailed unpaired t-test.

E Quantification of the proportion of short residences (< 120 s) and long residences (> 300 s) of Cse4^{CENP-A} alone or in ternary residences on CEN DNA. Short and long Non-Ternary^{Scm3} Cse4^{CENP-A} residences (0.69 and 0.08 respectively, n = 1,063 over three experiments of ~1,000 DNA molecules using different extracts) and short and long Ternary^{Scm3} Cse4^{CENP-A} residences (0.54 and 0.16 respectively, n = 305 over three experiments of ~1,000 DNA molecules using different extracts).

F Longer residence lifetimes are measured for Cse4^{CENP-A} after Scm3^{HJURP} colocalizes. Estimated survival function plots of Kaplan–Meier analysis of the lifetimes of Ternary^{Scm3} Cse4^{CENP-A} residences on CEN DNA (purple—median lifetime of 108 s, n = 305 over three experiments of ~1,000 DNA molecules using different extracts) and Non-Ternary^{Scm3} Cse4^{CENP-A} residences on CEN DNA (green—of 79 s, n = 1,230 over three experiments of ~1,000 DNA molecules using different extracts). Significant difference (**) between Ternary^{Scm3} and Non-Ternary^{Scm3} lifetime survival plots (two-tailed P-value of 2.1e-3 as determined by log-rank test). 95% confidence intervals indicated (dashed lines), right-censored lifetimes (plus icons) were included and unweighted in survival function estimates.

levels of Cse4^{CENP-A} in whole cell extracts (Fig EV4A). However, a short pulse of Scm3^{HJURP} overexpression did lead to a significant increase in the endpoint colocalization of Cse4^{CENP-A} on CEN DNA, while overexpression of Psh1 had the opposite effect (Fig EV4B and C). The median lifetime of Cse4^{CENP-A} on CEN DNA was also significantly increased when Scm3^{HJURP} was overexpressed and significantly decreased when Psh1 was overexpressed (Fig EV4D). These lifetime changes correlated with the propensity for Cse4^{CENP-A} to form ternary residences with Scm3^{HJURP} on the CEN DNA (Fig EV4E), suggesting they reflect changes in the availability of the complex. To assess if these perturbations to Cse4^{CENP-A} were consequential in cells, we grew cells under constant induction and found significant growth phenotypes when the Cse4^{CENP-A}-Scm3^{HJURP} complex was limited (Fig EV4F). These data indicate that Scm3^{HJURP} is limiting for stable centromeric nucleosome formation in our single molecule assembly assay and suggest that availability of the Cse4^{CENP-A}-Scm3^{HJURP} complex is likewise important for cell viability.

Stable Cse4^{CENP-A} association is blocked when centromere DNAs are tethered at both ends

Our observation of two subpopulations of Cse4^{CENP-A} molecules on CEN DNAs, including brief binders and longer-residing molecules that correlated with Scm3^{HJURP}, suggested a two-stage process for Cse4^{CENP-A} deposition that begins with transient, chaperone-independent targeting and is followed by chaperone-dependent stabilization. We hypothesized that the transition to more stable Cse4^{CENP-A} binding might require wrapping of the CEN DNA around the Cse4^{CENP-A}-containing histone octamer. If wrapping were indeed required for stabilization, then restricting the ability of the DNA to adopt a wrapped configuration should inhibit its stabilization on CEN DNA. To test this prediction, we created CEN DNA templates with biotins located at both ends to enable double-ended attachment to the coverslip surface. Tethering both ends of the template should limit its ability to twist or shorten, and thus to encircle a Cse4^{CENP-A} histone octamer, behaviors which are proposed to be essential for

Cse4^{CENP-A} nucleosome formation on centromeric DNA (Furuyama & Henikoff, 2009; Guo et al, 2021). To allow both ends to be tethered simultaneously to the coverslip surface, an additional biotin handle was introduced (instead of an organic dye) onto a shortened 250 bp version of the CEN DNA (Fig 4A). We first tested for a nucleosome-protected DNA fragment using a bulk assembly assay, in which template DNAs are linked to streptavidin-coated magnetic beads, incubated with cell extract to allow kinetochore assembly, and then washed, as done previously (Lang et al, 2018). In addition to the double-tethered template, controls using a single-tethered CEN template of the same length as well as a mutant CDEIII^{mut} template were also performed. After the assembly reactions, a mild micrococcal nuclease (MNase) digestion was performed to preferentially cut the unbound DNA in-between any assembled nucleosomes. Subsequent analysis of the DNA by gel electrophoresis showed strong protection of ~140 bp of the single-tether template, but almost no protection of the double-tethered template (Fig 4B). The CDEIII^{mut} template, which does not stably recruit Cse4^{CENP-A} (Lang et al, 2018), was completely unprotected as expected. Protection of the single-tether template was presumably due to formation of Cse4^{CENP-A}-containing nucleosomes, because this DNA fails to recruit H3 (Lang et al, 2018). These observations suggest that spatial restriction of the template can prevent Cse4 nucleosome assembly.

We next sought to analyze Cse4^{CENP-A} behavior on individual double-tethered CEN DNA templates in our TIRFM assay. Because the double tethered templates lacked an organic dye for visualization, we used Ndc10-mCherry as a fiducial marker for the CEN DNAs due to its high colocalization percentage (Fig 1C), rapid arrival, stable colocalization behavior, and our finding that most Cse4^{CENP-A} colocalizations occur after Ndc10 (Fig 2F and G). Endpoint colocalization of Cse4^{CENP-A} was reduced more than two-fold on the double-tethered CEN DNAs relative to single-tethered controls (Fig 4C and D). Likewise, time-lapse experiments (Fig 4E, Movie EV4) revealed that median Cse4^{CENP-A} residence lifetimes on double-tethered CEN DNAs were significantly shorter than on single-tethered templates (79 vs. 67 s, Fig 4F). Median lifetimes on single-tethered templates were comparable to those of the

Figure 4. Synthetic restriction of nucleosome formation severely restricts Cse4^{CENP-A} residence lifetimes on CEN DNA.

- A Schematic of single versus double-tether CEN DNA TIRFM colocalization assay.
- B Kinetochores were assembled on beads containing either a 250 bp single-tether, a 250 bp double-tether or a 250 bp CDEIII^{mut} CEN DNA. They were then treated with MNase, and the remaining DNA was visualized on an agarose gel. Black arrow indicates Cse4^{CENP-A} nucleosome protected DNA (~150 bp); white arrow indicates the theoretical location of undigested template DNA (250 bp).
- C Example images of TIRFM endpoint colocalization assays. Top panels show Cse4^{CENP-A}/Ndc10 ternary colocalizations visualized on single-tethered CEN DNA (top-left panel) or on double-tethered CEN DNA (top-right panel) with colocalization shown in relation to Ndc10 in yellow circles. Bottom panels show overlay of Ndc10 channel (magenta) with Cse4^{CENP-A} (green). Scale bars 3 μm.
- D Quantification of observed ternary colocalization of Cse4^{CENP-A} with Ndc10 (right) on single-tethered CEN DNA containing Ndc10 (19.9 ± 2.4%, avg ± s.d. n = 4 experiments, each examining ~1,000 DNA molecules from different extracts) and on double-tethered CEN DNA (7.3 ± 1.1%, avg ± s.d. n = 4 experiments, each examining ~1,000 DNA molecules from different extracts).
- E Representative residence lifetime assay traces of ternary Cse4^{CENP-A} residences with Ndc10 on single-tethered CEN DNA (top), double-tethered CEN DNA (middle) or of Cse4^{CENP-A} residence on CDEIII-80 bp CEN DNA (bottom). Each example includes kymographs of Cse4^{CENP-A} (488 nm-top) with normalized intensity trace (gray-bottom) as well as identified residences (blue). Images acquired every 5 s with normalized fluorescence intensity shown in arbitrary units.
- F Residence times for Cse4^{CENP-A} on double-tethered CEN DNAs are shorter than on single-tethered CEN DNAs and equivalent to those on non-functional mutant CEN DNAs. Estimated survival function plots of Kaplan–Meier analysis of ternary residences of Cse4^{CENP-A} with Ndc10 on single-tethered CEN DNA (blue—median lifetime of 79 s, n = 675 over three experiments of ~1,000 DNA molecules using different extracts), on double-tethered CEN DNA (red—median lifetime of 67 s, n = 3,175 over three experiments of ~1,000 DNA molecules using different extracts) or Cse4^{CENP-A} lifetimes on CDEIII-80 bp CEN DNA (purple—median lifetime of 71 s, n = 901 over three experiments of ~1,000 DNA molecules using different extracts). No significant difference (n.s.) between double-tethered 250 bp CEN DNA and 80 bp CDEIII CEN DNA lifetime survival plots (two-tailed P-value of 0.06 as determined by log-rank test). Significant difference (***) between double-tethered 250 bp CEN DNA and 250 bp single-tether DNA lifetime survival plots (two-tailed P-value of 1.4e-10 as determined by log-rank test). 95% confidence intervals indicated (dashed lines), right-censored lifetimes (plus icons) were included and unweighted in survival function estimates.

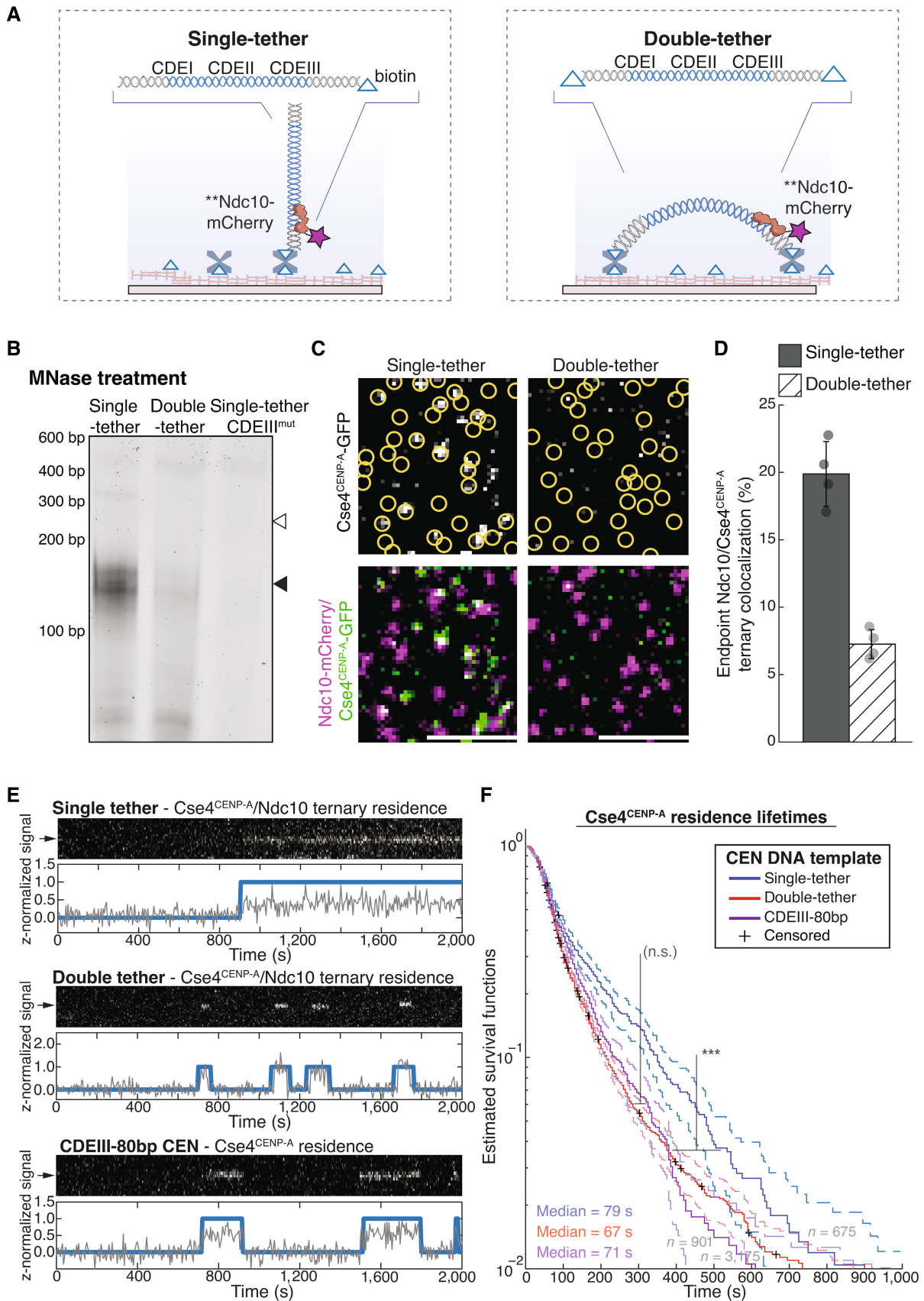


Figure 4.

previously measured ternary^{Ndc10} Cse4^{CENP-A} residences (79 vs. 88 s, Fig 4E and F, Table 1). But median lifetimes of Cse4^{CENP-A} on double-tethered templates were significantly shorter, and closer to non-ternary^{Ndc10} Cse4^{CENP-A} residences (67 vs. 69 s, Fig 4E and F, Table 1). As an alternative to physical restriction to prevent CEN DNA wrapping of Cse4^{CENP-A}, we designed a dye-labeled and single-tethered, severely truncated 80-bp template (CDEIII-80 bp CEN), that is too short to form a single wrap around the Cse4^{CENP-A}-containing core particle (Fig EV5A and B). Cse4^{CENP-A} residences were transient on CDEIII-80 bp CEN DNA (Fig EV5C) with a

shortened median lifetime that was comparable to the median lifetime of ternary residences on double-tethered templates (71 vs. 67 s, Figs 4E and F, and EV5D, Movie EV5). The median lifetimes of Cse4^{CENP-A} residences on either mutant CEN DNA (CDEIII-80 bp or double-tethered) were closer to the median lifetime of non-ternary^{Scm3} Cse4^{CENP-A} residences when compared to their ternary^{Scm3} counterparts (79 vs. 108 s). Thus, physical restriction of the CEN DNA template, either by shortening it or limiting its mobility, prevents stable association of Cse4^{CENP-A}, quantitatively reproducing the transient binding seen in the absence of either Ndc10 or the chaperone protein Scm3^{HJURP}. These observations suggest that stable deposition of Cse4 requires physical wrapping of the CEN DNA around the histone core, that both Ndc10 and Scm3^{HJURP} have an important role in the wrapping process, and that wrapping of centromeric DNA is a key kinetic hurdle in CEN nucleosome formation.

Table 1. Median survival times of protein residences determined from various conditions tested and reported in this study.

Protein	Context	50% Survival time (s)
Ndc10	Residences on CEN DNA	102
Cse4 ^{CENP-A}	Residences on CEN (in Ndc10-mCherry extract)	79
	Ternary ^{Ndc10} Cse4 ^{CENP-A} residences on CEN	88
	Non-Ternary ^{Ndc10} Cse4 ^{CENP-A} residences on CEN	69
	Residences on CEN3 (in Scm3 ^{HJURP} -mCherry extract)	82
	Residences on CEN7 (in Scm3 ^{HJURP} -mCherry extract)	74
	Residences on CEN9 (in Scm3 ^{HJURP} -mCherry extract)	78
	Ternary ^{Scm3} Cse4 ^{CENP-A} residences on CEN	108
	Non-Ternary ^{Scm3} Cse4 ^{CENP-A} residences on CEN	79
	Scm3 ^{HJURP} First—Ternary ^{Scm3} Cse4 ^{CENP-A} residences on CEN	108
	Scm3 ^{HJURP} Last—Ternary ^{Scm3} Cse4 ^{CENP-A} residences on CEN	133
Scm3 ^{HJURP}	Residences on CEN	61
	Residences on CDEIII ^{mut} CEN DNA	75
	Ternary ^{CENP-A} Scm3 ^{HJURP} residences on CEN	70
	Non-Ternary ^{CENP-A} Scm3 ^{HJURP} residences on CEN	63
Cse4 ^{CENP-A}	Residences on CDEIII ^{mut} CEN DNA	53
	Ternary ^{Scm3} Cse4 ^{CENP-A} residences on CDEIII ^{mut} CEN DNA	45
	Non-Ternary ^{Scm3} Cse4 ^{CENP-A} residences on CDEIII ^{mut} CEN DNA	52
	Residences on CEN (in pGAL-SCM3 extract)	101
	Residences on CEN (in pGAL-PSH1 extract)	53
	Ternary residences with Ndc10 on 250 bp single-tether CEN DNA	79
	Ternary residences with Ndc10 on 250 bp double-tether CEN DNA	67
	Residences on CDEIII-80 bp CEN DNA	71
	Residences on CEN (in <i>chl4-K13S</i> extract)	70
	Residences on CEN (in <i>okp1-AID</i> extract)	65

DNA-binding CCAN elements stabilize the centromeric nucleosome

Given the inherent instability of bare centromeric nucleosomes *in vitro* (Xiao *et al*, 2011; Dechassa *et al*, 2014), we hypothesized that additional stabilization after nucleosome formation might be provided by the binding of centromeric DNA-associated CCAN proteins. Such an additional stabilization step would explain our observations where Cse4^{CENP-A} and Scm3^{HJURP} colocalized together on CEN DNA without yielding long (> 300 s) Cse4^{CENP-A} residences (Fig 3E). To test this idea, we focused on two conserved CCAN proteins that recent structural studies showed interact with CEN DNA, Chl4^{CENP-N} and Okp1^{CENP-Q} (Yan *et al*, 2019; Guan *et al*, 2021). Although CENP-C also exhibits significant DNA association within the reconstitution of the human CCAN (Yatskevich *et al*, 2022), we chose not to target Mif2^{CENP-C} due to its absence from the yeast structural model. Chl4^{CENP-N} binds close to the Cse4^{CENP-A} nucleosome and forms a DNA-binding groove that binds the centromere and stabilizes an extended DNA section adjacent to the nucleosome (Fig 5A). Mutation of this Chl4^{CENP-N} DNA-binding groove (*chl4^{K13S}*) exhibits genetic interactions with mutants in Cse4^{CENP-A}, making it an ideal candidate to test its contribution to nucleosome stability (Yan *et al*, 2019). Okp1^{CENP-Q} forms a heterodimer with Ame1^{CENP-U} that has DNA binding activity and has been shown to interact with an N-terminal extension of Cse4^{CENP-A} within the nucleosome structure (Hornung *et al*, 2014; Hinshaw & Harrison, 2019; Yan *et al*, 2019) (Fig 5A). We therefore assayed Cse4^{CENP-A} endpoint colocalization in *chl4^{K13S}* and *okp1-AID* extracts and found that it was significantly impaired, even though total Cse4^{CENP-A} levels in the extracts were not significantly altered (Fig 5B–D). Cse4^{CENP-A} residence lifetimes in both *chl4^{K13S}* and *okp1-AID* extracts were also significantly reduced (Fig 5E and F). This disruption in centromeric nucleosome maintenance suggests that other kinetochore proteins that bind to CEN DNA also help to stabilize the nucleosome.

DNA composition of centromeres contributes to genetic stability through Cse4^{CENP-A} recruitment

We next sought to investigate the role of centromeric DNA sequence in centromeric nucleosome formation since it has been difficult to reconstitute stable centromeric nucleosomes *in vitro* (Dechassa *et al*, 2011; Yan *et al*, 2019; Guan *et al*, 2021). To do so, we took

advantage of earlier work, where a synthetic library of centromeric DNAs with randomized CDEII sequences was screened for members that can functionally replace native centromeres *in vivo*. This screen revealed that synthetic centromere function correlates strongly with high homopolymeric A + T content, defined as continuous “runs” of four or more A or T residues ($A_n \geq 4$ or $T_n \geq 4$), within CDEII (Baker & Rogers, 2005). Synthetic centromeres in which a high fraction of CDEII residues (> 0.38) occurred in runs of $A_n \geq 4$ or $T_n \geq 4$ were genetically more stable than synthetic centromeres with lower

fractions of homopolymeric A + T runs within CDEII (< 0.38), although all chromosomes with synthetic centromeres were less stable *in vivo* when compared to a WT centromere. We therefore refer to the synthetic centromeres with more AT runs as “unstable” and those with less AT runs as “very unstable” mutants (Fig 6A). To test whether these differences in CDEII sequence and genetic stability correlate with the ability of the templates to retain Cse4^{CENP-A}, we performed endpoint colocalization assays, using two unstable and two very unstable mutant CEN DNAs (Baker & Rogers, 2005). While

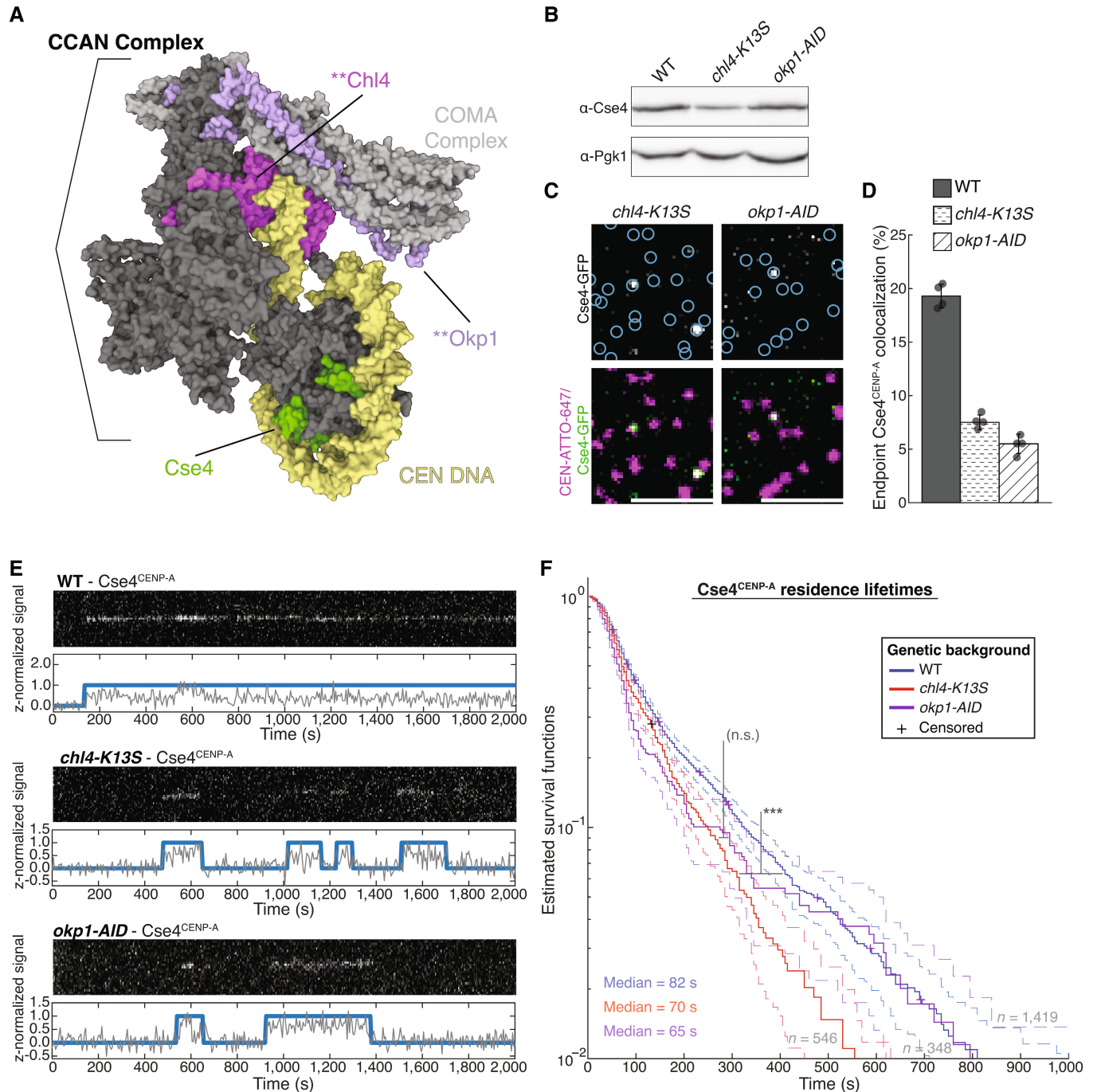


Figure 5.

Figure 5. DNA-binding CCAN proteins stabilize the nucleosome to provide a platform for kinetochore assembly.

- A Structure of the yeast CCAN in complex with Cse4^{CENP-A} with CEN DNA (yellow), Cse4^{CENP-A} (green), Chl4^{CENP-N} (magenta) and Okp1^{CENP-Q} (purple), highlighting DNA-adjacent regions targeted by the *chl4-K13S* mutant or proteasomal degradation of Okp1^{CENP-Q} (*okp1-AID*). Image of 6QLD (Yan et al, 2019) created with Mol* (Sehnal et al, 2021).
- B Immunoblot analysis of whole cell extracts from WT, *chl4-K13S* and *okp1-AID* cells using indicated antibodies.
- C Example images of TIRFM endpoint colocalization assays. Top panels show visualized Cse4^{CENP-A}-GFP on CEN DNA in extracts from *chl4-K13S* (top-left panel) or auxin-treated *okp1-AID* strains (*okp1-AID*, top-right panel) with colocalization shown in relation to identified CEN DNA in blue circles. Bottom panels show overlay of CEN DNA channel (magenta) with Cse4^{CENP-A}-GFP (green). Scale bars 3 μm.
- D Quantification of Cse4^{CENP-A} endpoint colocalization with CEN DNA in extracts from WT, *chl4-K13S*, or *okp1-AID* genetic backgrounds (19 ± 1.1%, 8 ± 0.7%, 5 ± 0.9%, avg ± s.d. n = 4 experiments, each examining ~1,000 DNA molecules from different extracts).
- E Representative residence traces of Cse4^{CENP-A} signal on CEN DNA in WT (top), *chl4-K13S* (middle), or *okp1-AID* (bottom) extracts. Each example includes kymographs of Cse4^{CENP-A} (488 nm-top) with normalized intensity trace (gray-bottom) as well as identified residences (blue). Images acquired every 5 s with normalized fluorescence intensity shown in arbitrary units.
- F Kaplan–Meier analysis of Cse4^{CENP-A} residence lifetimes on CEN DNA in extracts from WT (blue—median lifetime of 82 s, n = 1,419 over three experiments of ~1,000 DNA molecules using different extracts), *chl4-K13S* (red—median lifetime of 70 s, n = 546 over three experiments of ~1,000 DNA molecules using different extracts) and *okp1-AID* (purple—median lifetime of 61 s, n = 348 over three experiments of ~1,000 DNA molecules using different extracts) genetic backgrounds. Significant difference (***) between WT extract and *chl4-K13S* extract residence lifetime plots (two-tailed P-value of 3.4e-5 as determined by log-rank test). No significant difference (n.s.) between *chl4-K13S* and *okp1-AID* residence lifetimes in (two-tailed P-value of 0.40 as determined by log-rank test). 95% confidence intervals indicated (dashed lines), right-censored lifetimes (plus icons) were included and unweighted in survival function estimates.

all four mutants recruited lower levels of Cse4^{CENP-A} compared to WT CEN DNA, the unstable mutants recruited higher levels of Cse4^{CENP-A} than their very unstable counterparts (Fig 6B and C), and Cse4^{CENP-A} recruitment levels across the different templates correlated strongly with the fraction of CDEII residues in homopolymeric A + T runs (Fig 6D) and with the stability of chromosome inheritance *in vivo* (Fig 6D, inset). Time-lapse experiments with the same four mutants showed that the average number of Cse4^{CENP-A} residences observed per CEN DNA in a 45 min imaging sequence also correlated with homopolymeric A + T run content and CEN functionality *in vivo* (Fig 6E, left). This relationship was apparently independent of Scm3^{HJURP}, because the average number of Scm3^{HJURP} residences observed per CEN DNA remained consistent across the mutants (Fig 6E, right). Consistent with this Scm3^{HJURP}-independent behavior, the proportion of ternary Cse4^{CENP-A}-Scm3^{HJURP} residences was similar in “very unstable” CDEII mutant CEN DNA when compared to CEN DNA (Appendix Fig S3A), but there was a significant increase in the estimated off-rates of ternary^{Scm3} Cse4^{CENP-A} residences on “very unstable” CDEII mutant CEN DNA (Appendix Fig S3B). These results suggest that despite not affecting Scm3^{HJURP}-Cse4^{CENP-A} ternary residence initiation, very unstable CDEII mutants might restrict Scm3^{HJURP}-catalyzed stabilization of Cse4^{CENP-A}.

To further explore the role of DNA sequence, we generated several other templates that maintained high percentages of A and T residues (high % A/T) yet had very little homopolymeric A_{n ≥ 4} or T_{n ≥ 4} run content. A CDEII mutant that contained a substitution of satellite DNA from human chromosomes (α-sat) failed to recruit stable Cse4^{CENP-A} in endpoint colocalization assays despite its high % A/T (Fig 6D). The hybrid sequence combining CDEIII and Widom 601 (Widom-601-hybrid) that readily forms centromeric nucleosomes in recombinant reconstitutions (Yan et al, 2019) (Appendix Fig S4A) also failed to recruit stable Cse4^{CENP-A} in endpoint colocalization assays (Fig 6D). To ensure that the Widom-601-hybrid CEN DNA was not saturated by the canonical H3 histone, we also monitored H3 incorporation. The Widom-601-hybrid CEN DNA incorporated low levels of H3, similar to WT CEN DNA, in both bulk assembly assays (Appendix Fig S4B) and endpoint colocalization assays (Appendix Fig S4C and D). Such low levels of H3 incorporation were unexpected, as Widom-601 readily forms stable H3 nucleosomes when reconstituted (Lowary & Widom, 1998), but this may

point to differences in *de novo* histone formation that have yet to be fully studied. Removal of the CDEIII sequence from the Widom-601-hybrid to prevent CBF3 binding yielded an approximately two-fold increase in H3 incorporation (Appendix Fig S4C and D), suggesting that CBF3 may negatively regulate H3 binding at centromeres. Taken together, these data highlight a critical functional role for homopolymeric A + T run content within CDEII for stable Cse4^{CENP-A} recruitment.

Discussion

Here, we report adaptation of a cell-free system to autonomously assemble native centromeric nucleosomes on individual centromeric DNA molecules with CoSMoS to enable the study of native centromeric nucleosome formation at spatiotemporal resolutions not previously accessible. Continuous monitoring revealed that several cofactors coordinate to promote stable Cse4^{CENP-A} recruitment and maintenance at the centromere. These cofactors include the DNA-binding CBF3 component Ndc10, as well as the conserved chaperone Scm3^{HJURP}. We found that Scm3^{HJURP} was a limiting cofactor that promoted stable centromeric Cse4^{CENP-A} association but was not required for transient centromere association. Stabilization of Cse4^{CENP-A} likely occurred through catalysis of centromeric DNA wrapping because we observed that physical restriction of the DNA impaired stable recruitment of Cse4^{CENP-A}. Guided by recent structural kinetochore reconstitutions (Yan et al, 2019; Guan et al, 2021), we also found that the centromeric nucleosome must be stabilized by DNA-associated kinetochore proteins within the CCAN, highlighting the tight coordination of kinetochore assembly at the inner kinetochore. This finding may in part explain the instances where Cse4^{CENP-A} colocalized on CEN DNA with its chaperone Scm3^{HJURP} yet failed to remain stably associated. In those instances, the Cse4^{CENP-A} nucleosome may have successfully formed, but subsequent association of CCAN kinetochore proteins failed to occur, permitting dissolution of the nucleosome complex (Fig 7). We also interrogated the CDEII DNA element and identified a role for sequence composition in stable centromeric nucleosome recruitment which correlated with centromere stability in cells. Taken together, this assay enabled the assessment at high resolution

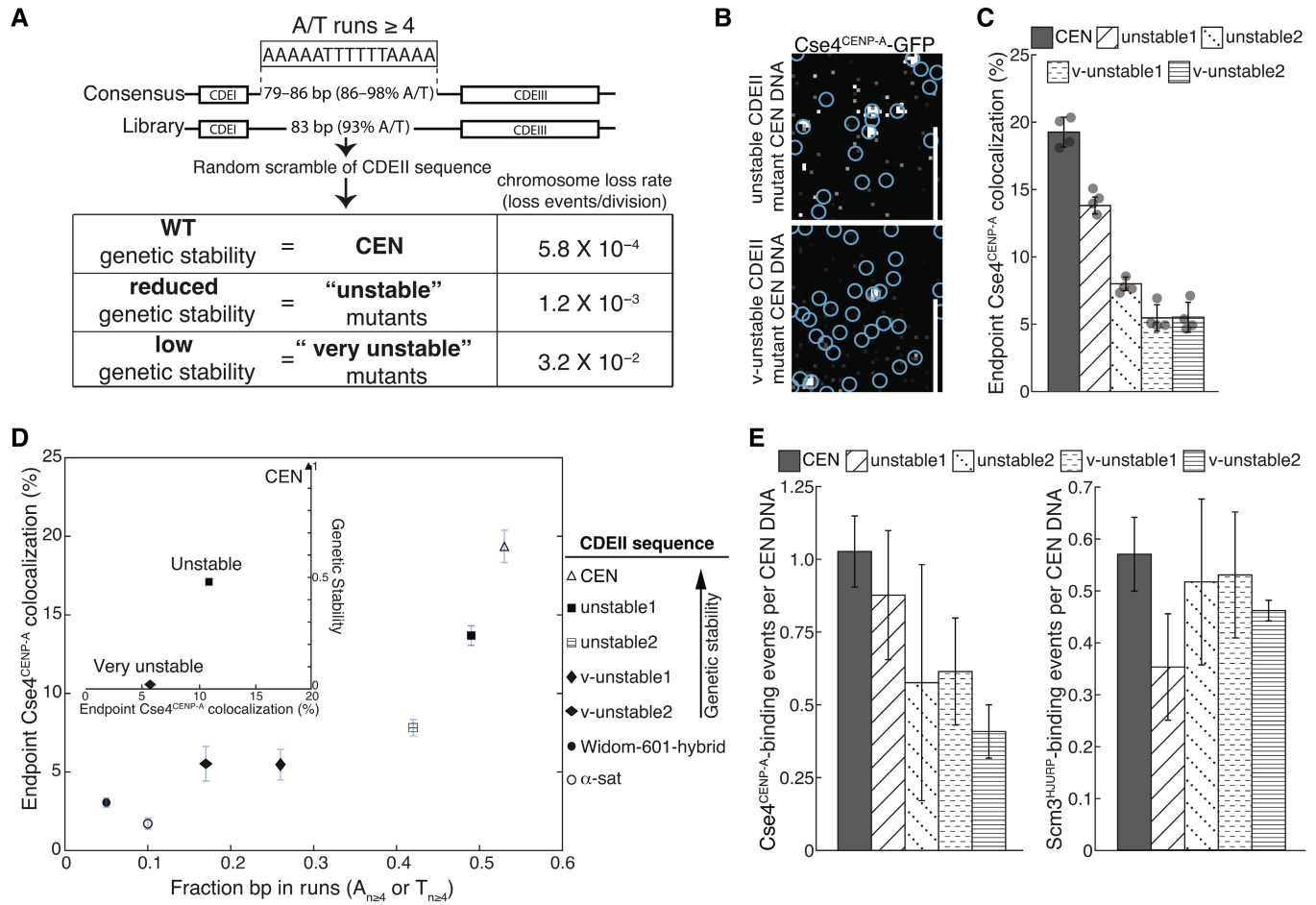


Figure 6. DNA-composition of centromeres contributes to genetic stability through Cse4^{CENP-A} recruitment.

A Overview of CDEII mutants generated for stability assays where overall % of A/T content was maintained while A/T run content was randomly varied and selected for genetic stability including reported chromosome loss rates of WT and CDEII mutant pools (adapted from Baker & Rogers, 2005).

B Example images of TIRFM endpoint colocalization assays. Visualized Cse4^{CENP-A}-GFP on unstable1 CDEII-mutant DNA (top panel) or on v-unstable1 CDEII-mutant DNA (bottom panel) with colocalization shown in relation to identified CEN DNA in blue circles. Scale bars 3 μ m.

C Quantification of endpoint colocalization of Cse4^{CENP-A} on CEN, unstable1, unstable2, v-unstable1, and v-unstable2 CEN DNA (19.3 \pm 1.1%, 13.8 \pm 0.6%, 7.8 \pm 0.5%, 5.5 \pm 1.0%, 5.5 \pm 1.1%, avg \pm s.d. n = 4 experiments, each examining \sim 1,000 DNA molecules from different extracts).

D Stable Cse4^{CENP-A} recruitment depends upon CDEII sequence A/T run content. Plot of fraction of all CDEII bp that occur in homopolymeric A_{n \geq 4} or T_{n \geq 4} repeats (fraction bp in runs, $N \geq 4$) in CEN, unstable1, unstable2, v-unstable1, v-unstable2, Widom-601 hybrid and α -sat CEN DNA (0.53, 0.49, 0.41, 0.26, 0.17, 0.05, 0.10), versus the observed colocalization of Cse4^{CENP-A} on CEN, unstable1, unstable2, v-unstable1, v-unstable2, Widom-601 hybrid and α -sat CEN DNA (19.3 \pm 1.1%, 13.8 \pm 0.6%, 7.8 \pm 0.5%, 5.5 \pm 1.0%, 5.5 \pm 1.1%, 3.1 \pm 0.3%, 1.7 \pm 0.4%, avg \pm s.d. n = 4). Inset plot of Cse4^{CENP-A} endpoint colocalization percentage on CEN, unstable mutants (average), and very unstable mutants (average) (19.9, 10.8, and 5.5% respectively) versus genetic stability (chromosome loss normalized to CEN) of WT, unstable mutants, and very unstable mutants (1.0, 0.48, and 0.02, respectively).

E Very unstable CDEII mutants have reduced average Cse4^{CENP-A} binding when compared to unstable counterparts. Average residences of Cse4^{CENP-A} per CEN DNA (left) on CEN, unstable1, unstable2, v-unstable1, and v-unstable2 CEN DNA (1.03 \pm 0.12, 0.88 \pm 0.22, 0.58 \pm 0.41, 0.61 \pm 0.18, 0.41 \pm 0.09, avg \pm s.e.m. n = 3 experiments of \sim 1,000 DNA molecules using different extracts) and average residences of Scm3^{HJURP} per CEN DNA (right) on CEN, unstable1, unstable2, v-unstable1, and v-unstable2 CEN DNA (0.57 \pm 0.07, 0.35 \pm 0.10, 0.52 \pm 0.16, 0.53 \pm 0.12, 0.46 \pm 0.02, avg \pm s.e.m. n = 3 experiments of \sim 1,000 DNA molecules using different extracts).

of the native nucleosome assembly process on centromeric DNA as well as a functional role of centromere DNA sequence composition.

Formation of a native centromeric nucleosome

Despite over a decade of ongoing study, reconstituting Cse4^{CENP-A} nucleosomes with yeast centromeric DNA has remained remarkably elusive. Recent structural studies have started to shed light on these

complexes, yet there are fundamental differences between these reconstitutions and native kinetochore assemblies. One such example is our finding that the Widom 601-hybrid sequence that readily stabilized the Cse4^{CENP-A} nucleosome *in vitro* was a poor template for Cse4^{CENP-A} recruitment and stable nucleosome formation *de novo* (Fig 6E). Structural models using non-native CEN DNA required significant rearrangements around the centromeric nucleosome to permit CCAN assembly, including dissociation of the CBF3

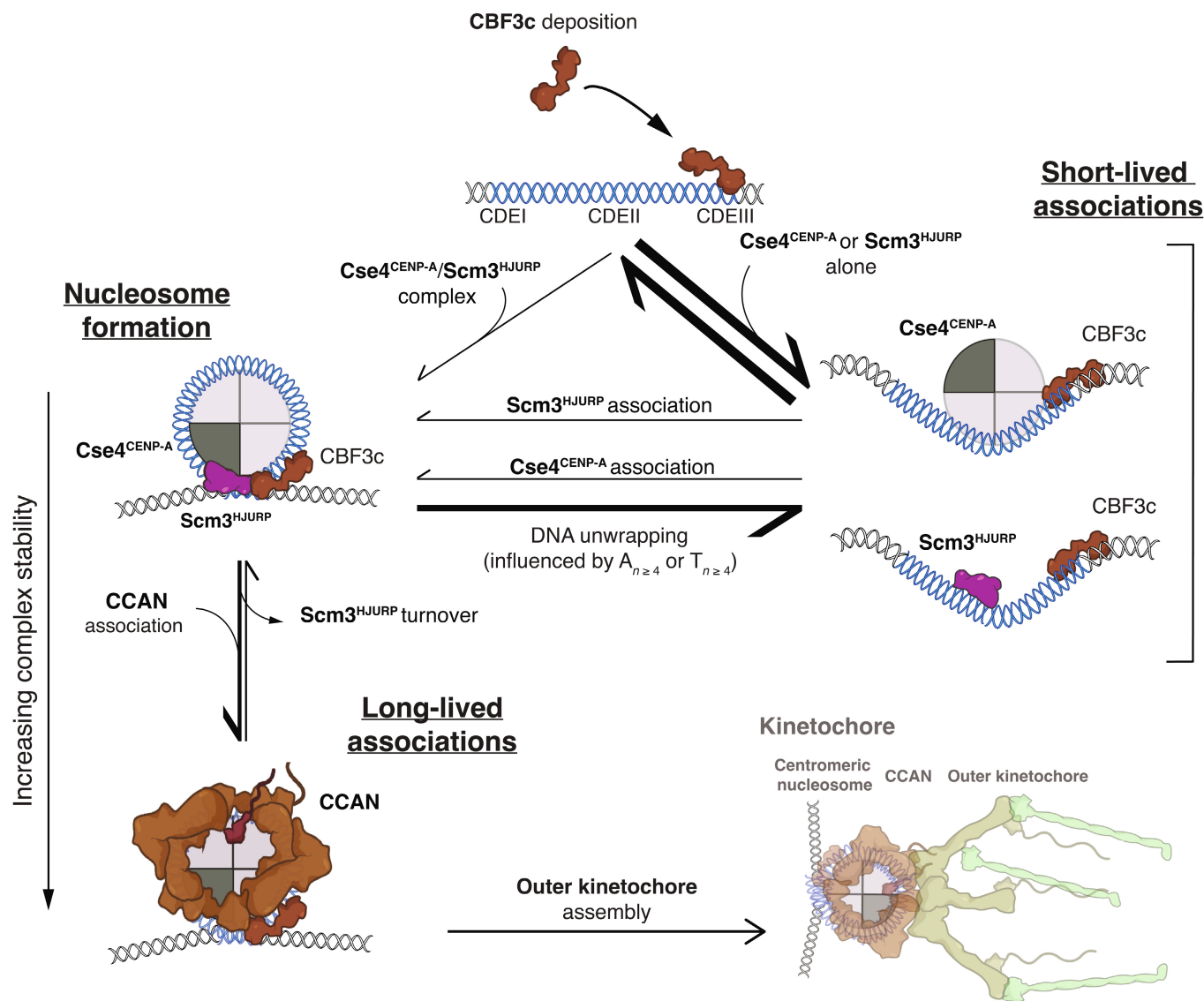


Figure 7. Formation of stable centromeric nucleosome requires tight coordination of centromeric DNA, Cse4^{CENP-A} with its chaperone Scm3^{HJURP} and CCAN kinetochore protein association.

Schematic of centromeric nucleosome formation highlighting the different pathways that could lead to either short-lived or long-lived residences Cse4^{CENP-A} as measured in TIRFM resident lifetime assays.

complex (Yan *et al*, 2019; Guan *et al*, 2021). However, we did not observe a significant reduction in CBF3 complex colocalization, even after sufficient incubation to allow full *de novo* kinetochore assembly (Lang *et al*, 2018). Our findings are consistent with observed CBF3 behavior in cells (Joglekar *et al*, 2008) and highlight both the potential significant differences between *in vitro* reconstitutions of kinetochore complexes and their native counterparts as well as the significant advantage of assembling kinetochores under native conditions.

Our work suggests the major functional role of the Scm3^{HJURP} chaperone at centromeres may be Cse4^{CENP-A} incorporation into stable nucleosomes instead of centromere targeting (Camahort *et al*, 2007; Cho & Harrison, 2011b). We found that Scm3^{HJURP} is a

limiting kinetochore assembly factor required to catalyze stable Cse4^{CENP-A} recruitment (Figs 3, 4 and EV4). The population of Cse4^{CENP-A} that localized to CEN DNA in the absence of Scm3^{HJURP} was presumably bound to other chaperone proteins it is known to associate with, such as CAF-1, Spt6, and DAXX (Lacoste *et al*, 2014; Hewawasam *et al*, 2018; Bobkov *et al*, 2020). It should be acknowledged that it is possible that transient Cse4^{CENP-A} binding may be driven in some part through mass action due to high concentrations of CEN DNA and *in vivo*, this transient binding may not be physiologically relevant. However, our data shows that these associations are insufficient for stable nucleosome formation in the absence of Scm3^{HJURP}. Given that physical restriction of DNA wrapping severely limited stable association of Cse4^{CENP-A} (Fig 4), we further

propose that Scm3^{HJURP} promotes stable Cse4^{CENP-A} recruitment through catalysis of centromeric DNA wrapping, consistent with its activity *in vitro* (Dechassa et al, 2011; Xiao et al, 2011). While several chaperones have been shown to limit ectopic Cse4^{CENP-A} deposition (Ranjitkar et al, 2010; Gkikopoulos et al, 2011; Hewawasam et al, 2018), it is likely that Scm3^{HJURP} promotes specific deposition at centromeres through two non-exclusive mechanisms: (i) tethering of Cse4^{CENP-A} via Scm3^{HJURP}-Ndc10 binding to promote centromeric DNA wrapping and (ii) stabilization of a Cse4^{CENP-A}-centromere DNA intermediate through the AT-rich DNA binding domain of Scm3^{HJURP} (Xiao et al, 2011). While we aim to further investigate this mechanism, either possibility yields a model of Scm3^{HJURP}-catalyzed Cse4^{CENP-A} nucleosome formation that is supported by *in vitro* reconstitutions, where it was found that Scm3^{HJURP} was required to form a Cse4^{CENP-A} nucleosome on the highly AT-rich (and thus inherently unfavorably for histone wrapping) centromeric DNA (Dechassa et al, 2011; Xiao et al, 2011). In addition, this model is consistent with *in vivo* studies that showed Scm3^{HJURP} coordinates with Ndc10 to deposit Cse4^{CENP-A} at the centromere and is persistent at centromeres after Cse4^{CENP-A} deposition, although undergoing rapid exchange (Xiao et al, 2011; Wisniewski et al, 2014).

A functional role for the essential centromere element CDEII

The single molecule TIRFM colocalization assays developed here enabled direct assessment of a functional role of the centromeric CDEII element, a question that has been extremely difficult to address *in vivo*. While there is no sequence conservation across CDEII elements in yeast, they are often among the loci with the highest A/T % across the genome (Baker & Rogers, 2005). Although high A/T % is not a universal feature of all centromeres (Melters et al, 2013), it is a widely conserved feature across centromeres in both yeast and higher organisms despite being unfavorable for core histone wrapping (Struhl & Segal, 2013). Our work uncovered a role for CDEII sequence composition in stable Cse4^{CENP-A} nucleosome recruitment and suggests that homopolymeric A + T run content contributes to stable incorporation of Cse4^{CENP-A}. The requirement for A + T run content is highlighted by the failure of the canonical nucleosome-targeting Widom 601-based centromere (Widom 601-hybrid), which has high A/T% but contains little A + T run content, to stably recruit Cse4^{CENP-A} in our assay (Fig 6E), despite readily forming in reconstitutions (Xiao et al, 2011). This points to potentially significant differences in the formation of native centromeric complexes and their recombinant counterparts. In addition, it remains an open question whether yeast CDEII element sequences have evolved to maximize Cse4^{CENP-A} recruitment and stability or have evolved to a point where Cse4^{CENP-A} stability is sufficient to maintain centromere identity, as no A + T run beyond 8 nucleotides occurs within CDEII sequences despite occurring outside of centromeric loci (Baker & Rogers, 2005). Organisms with more complex centromeric architectures that maintain high A/T% fail to substitute for CDEII function in yeast centromeres, likely due to the lack of high A + T run content (Fig 6E).

Our work also supports a previously proposed model where A/T-rich centromeric DNA functions to restrict canonical histone formation (Drew & Travers, 1985; Xiao et al, 2011; Dechassa et al, 2014; Stormberg & Lyubchenko, 2022). This model is consistent with findings in other organisms where H3 histone eviction was an inherent property of

centromeric DNA and with our own findings that H3 has low occupancy on the CEN templates (Baker & Rogers, 2005; Shukla et al, 2018). This potential functional role of centromere sequence and/or centromere-binding kinetochore proteins in H3-eviction may be providing a drive to the genetic conservation of AT-rich DNA among centromere sequences. We speculate that in yeast, additional DNA-binding kinetochore proteins arose to aid in overcoming this kinetic barrier and to protect centromere function. This may be a consequence of the fact that despite a lack of meiotic drive, yeast centromeres are among the fastest evolving regions of the yeast genome and are thus sensitive to negative selection resulting in complete loss of centromere identity (Bensasson et al, 2008). Rapid purifying selection may also explain the accumulation of homopolymeric A + T run content within CDEII, which we found correlated to stable Cse4^{CENP-A} recruitment. This was somewhat unexpected, as homopolymeric repeats were found to resist nucleosome formation (Liebl & Zacharias, 2021). However, it has been reported that stretches of A-repeats impose a net curvature into dsDNA and that the DNA bend at centromeres contributes to their stability in cells (Murphy et al, 1991; Beutel & Gold, 1992; Widom, 2001). We therefore propose that homopolymeric A + T runs are cooperative with additional DNA-associated kinetochore proteins to facilitate nucleosome stability and kinetochore assembly and may explain the observed requirement for the A/T-rich DNA-binding Scm3^{HJURP} to catalyze centromeric DNA wrapping of Cse4^{CENP-A} (Figs 3 and 4). The precise mechanism by which these A + T runs contribute to nucleosome formation remains open for further study, but at the very least may provide context for the required coordination of several DNA-binding proteins that are in close proximity to the Cse4^{CENP-A} nucleosome (Fig 7).

Adaptation of the assay developed here to study downstream kinetochore assembly will enable the study of the contributions of various kinetochore proteins from within the vast network required to form a functional kinetochore scaffold. This assay may also be adapted to study the dynamics of other histones and chaperones as well as to further recapitulate a native centromere “cell-like” environment by including processes such as centromere replication, which precludes kinetochore assembly in cells (Furuyama & Biggins, 2007; Gkikopoulos et al, 2011; Bobkov et al, 2020). In addition, templates that include more complex chromatin structures surrounding the centromere that may provide additional information about the roles pericentromeric chromatin plays in maintenance of centromere identity and function. Such adaptations may be needed to better understand how such an initially tenuous assembly pathway with stringent prerequisite conditions occurs so rapidly and with such fidelity in cells throughout passage of every cell cycle. The mechanisms that drive this process and that may be abrogated in various cellular disease states are a critical area of study.

Materials and Methods

Yeast methods

The *S. cerevisiae* strains used in this study are listed in Appendix Table S1 and are derivative of SBY3 (W303). Standard genetic crosses, media, and microbial techniques were used. Cse4 was tagged internally at residue 80 with eGFP including linkers on either side (pSB1617) and then expressed from its native promoter at an

exogenous locus in a *cse4Δ* background (SBY19926). Genes that were changed to include endogenously tagged fluorescent protein alleles (mCherry) or epitope tags (-13myc) or auxin-inducible degrons (-IAA7) were constructed at the endogenous loci by standard PCR-based integration techniques (Longtine *et al*, 1998) and confirmed by PCR. The mutant *chl4-K13S* was made via PCR-based integration from a vector (pSB2182) containing the *CHL4* gene with 13 mutations present (Yan *et al*, 2019). The plasmids and primers used to generate strains are listed in Appendix Tables S2 and S3, respectively. All liquid cultures were grown in yeast peptone dextrose rich (YPD) media. To arrest cells in mitosis, log phase cultures were diluted in liquid media to a final concentration of 30 μg/ml benomyl and grown for another 3 h until at least 90% of cells were large-budded. For strains with auxin inducible degron (AID) alleles (*scm3-AID*, *okp1-AID*), all cultures used in the experiment were treated with 500 μM indole-3-acetic acid (IAA, dissolved in DMSO) for the final 60 min of growth as described previously (Nishimura *et al*, 2009; Miller *et al*, 2016; Lang *et al*, 2018). For strains with galactose inducible alleles (*pGAL-PSH1*, *pGAL-SCM3*), cultures were grown in raffinose and then treated with 4% galactose for the final 60 min of growth. Growth assays were performed by diluting log phase cultures to OD600 ~ 1.0 from which a 1:5 serial dilution series was made. This series was plated on YPD and YP plates that contained 4% Galactose and incubated at 23°C.

Preparation of DNA templates and Dynabeads

Plasmid pSB963 was used to generate the WT CEN DNA templates and pSB972 was used to generate the CEN^{mut} template used in this study. Derivatives of pSB963 were altered using mutagenic primers and Q5 site-directed mutagenesis kit (NEB) to generate vectors containing CEN9, unstable 1, unstable 2, very unstable 1, very unstable 2, α-sat, and 80 bp-CDEIII sequences (pSB3338, pSB3336, pSB3416, pSB3337, pSB3415, and pSB3335, respectively). CDEII mutants were taken directly from high-loss and low-loss pools from Baker & Rogers (2005) where very unstable 1 is equivalent to H1, very unstable 2 is equivalent to H14, unstable 1 is equivalent to L1, and unstable 2 is equivalent to L5. Widom-601 template was equivalent to the one used in structural studies (Guan *et al*, 2021) where CENIII (92–137) was inserted into corresponding region of 601 sequence (pSB3264). For α-sat CEN DNA, the CDEII region of the CEN template was mutated to a fragment of α-satellite DNA from *H. sapiens* X-chromosome based on structural studies containing CENP-A (Yatskevich *et al*, 2022). DNA templates were generated by PCR using a 5'-ATTO647-functionalized (IDT DNA) 5' primer with homology to linker DNA upstream of ~60 bp of pericentromeric DNA and the centromere (SB7843) and a 5'-biotinylated (IDT DNA) 3' primer with linker DNA, an EcoRI restriction site, and homology to linker DNA downstream of ~60 bp of pericentromeric DNA and the centromere (SB3879) to yield ~750 bp dye-labeled assembly templates. For the 80 bp CDEIII mutant, plasmid pSB963 was amplified with primers SB7843 and SB7844 to generate a CDEIII-containing mutant of 80 bp total length. For CEN7, template pSB2953 was amplified with primers SB5699 and SB7842 to generate a dye-labeled and biotinylated 750 bp assembly template. For the double-tethered CEN DNA template, biotinylated primers SB7845 and SB3878 were used to generate a 250 bp template. The single-

tethered 250 bp control template was generated using primers SB7846 and SB3878. The Widom-601 template (pSB2887) and Widom-601-CDEIII hybrid template (pSB3264) were amplified with primers SB5699 and SB7842 to generate dye-labeled and biotinylated 750 bp templates. Appendix Table S2 includes the plasmids used in this study and Appendix Table S3 includes the primer sequences used to PCR amplify the DNA templates. PCR products were purified using the Qiagen PCR Purification Kit. In the case of bulk assembly for MNase assays, purified CEN DNA was conjugated to Streptavidin-coated Dynabeads (M-280 Streptavidin, Invitrogen) for 2.5 h at room temperature, using 1 M NaCl, 5 mM Tris-HCl (pH7.5), and 0.5 mM EDTA as the binding and washing buffer. For single molecule TIRFM assays, purified DNA was diluted in dH₂O to a final concentration ~100 pM.

Whole cell extract preparation for kinetochore assembly assays

For a standard bulk kinetochore assembly assay *in vitro*, cells were grown in liquid YPD media to log phase and arrested in mitosis in 500 ml and then harvested by centrifugation. All subsequent steps were performed on ice with 4°C buffers. Cells were washed once with dH₂O with 0.2 mM PMSF, then once with Buffer L (25 mM HEPES pH 7.6, 2 mM MgCl₂, 0.1 mM EDTA pH 7.6, 0.5 mM EGTA pH 7.6, 0.1% NP-40, 175 mM K-Glutamate, and 15% Glycerol) supplemented with protease inhibitors (10 mg/ml leupeptin, 10 mg/ml pepstatin, 10 mg/ml chymostatin, 0.2 mM PMSF), and 2 mM DTT. Cell pellets were then snap frozen in liquid nitrogen and then lysed using a Freezer/Mill (SPEX Sample-Prep), using 10 rounds that consisted of 2 min of bombarding the pellet at 10 cycles per second, then cooling for 2 min. The subsequent powder was weighed and then resuspended in Buffer L according to the following calculation: weight of pellet (g) × 2 = number of ml of Buffer L. Resuspended cell lysate was thawed on ice and clarified by centrifugation at 16,100 g for 30 min at 4°C, the protein-containing layer was extracted with a syringe and then aliquoted and snap frozen in liquid nitrogen. The resulting soluble whole cell extracts (WCE) generally had a concentration of 50–70 mg/ml. The pellets, powder, and WCE were stored at –80°C.

Bulk assembly assays followed by MNase treatment

De novo kinetochore assembly was performed with whole cell extract from SBY21110 (Ndc10-mCherry, Cse4-GFP) as previously described (Lang *et al*, 2018). Briefly, 1 ml of whole cell extract and 50 μl of DNA coated M280 Dynabeads (single-tether CEN, double-tether CEN, or CEN^{mut}) were incubated at room temperature for 90 min to allow kinetochore assembly. Following the final wash, beads were resuspended in 90 μl of Buffer L (see above) supplemented with 100 μg/ml BSA, 10 μl of 10× Micrococcal Nuclease Reaction Buffer (NEB) and 1,000 gel units of Micrococcal Nuclease (NEB, #M0247S) and incubated at 30°C for 10 min under constant mixing. The reaction was stopped with addition of EGTA to 10 mM. After removal of magnetic beads, the aqueous phase was phenol-extracted followed by ethanol precipitation of DNA and resuspended in dH₂O and run on a 1% agarose gel. Resolved DNA were visualized via SYBR Gold nucleic acid dye (Invitrogen; S11494) on ChemiDoc Imager (Bio-Rad).

Immunoblotting

For immunoblots, proteins were transferred from SDS-PAGE gels onto 0.22 μM cellulose paper, blocked at room temperature with 4% milk in PBST, and incubated overnight at 4°C in primary antibody. Antibody origins and dilutions in PBST were as follows: α -Cse4 (9536; Pinsky *et al.*, 2003; 1:500), α -H3 Alexa Fluor 555 (Invitrogen; 17H2L9; 1:3,000), α -Pgk1 (Invitrogen; 4592560; 1:10,000). The anti-Scm3 antibodies were generated in rabbits against a recombinant Scm3 protein fragment (residues 1–28) of the protein by Genscript. The company provided affinity-purified antibodies that we validated by immunoprecipitating Scm3 from yeast strains with Scm3-V5 and confirming that the antibody recognized a protein of the correct molecular weight that was also recognized by α -V5 antibody (Invitrogen; R96025; 1:5,000). We subsequently used the antibody at a dilution of 1:10,000. Secondary antibodies were validated by the same methods as the primary antibodies as well as with negative controls lacking primary antibodies to confirm specificity. Blots were then washed again with PBST and incubated with secondary antibody at room temperature. Secondary antibodies were α -mouse (NA931) or α -rabbit (NA934), horseradish peroxidase-conjugated purchased from GE Healthcare and used at 1:1,000 dilution in 4% milk in PBST. Blots were then washed again with PBST and ECL substrate from Thermo Scientific used to visualize the proteins on ChemiDoc Imager (Bio-Rad). Uncropped and unprocessed scans of gels and blots are provided in the associated Source Data files.

Single molecule TIRFM slide preparation

Coverslips and microscope slides were ultrasonically cleaned and passivated with PEG as described previously (Larson *et al.*, 2014; Larson & Hoskins, 2017). Briefly, ultrasonically cleaned slides were treated with vectabond (Vector Laboratories) prior to incubation with 1% (w/v%) biotinylated mPEG-SVA MW-5000K/mPEG-SVA MW-5000K (Lysan Bio) in flow chambers made with double-sided tape. Passivation was carried out overnight at 4°C. After passivation, flow chambers were washed with Buffer L and then incubated with 0.3 M BSA/0.3 M Kappa Casein in Buffer L for 5 min. Flow chambers were washed with Buffer L and then incubated with 0.3 mg/ml Avidin DN (Vector Laboratories) for 5 min. Flow chambers were then washed with Buffer L and incubated with ~ 100 pM CEN DNA template for 5 min and washed with Buffer L. For endpoint colocalization assays, slides were prepared as follows: Flow chambers were filled with 100 μl of WCE containing protein(s) of interest via pipetting and wicking with filter paper. After addition of WCE, slides were incubated for 90 min at 25°C and then WCE was washed away with Buffer L. Flow chambers were then filled with Buffer L with oxygen scavenger system (Aitken *et al.*, 2008) (10 nM PCD/2.5 mM PCA/1 mM Trolox) for imaging. For immunofluorescence of H3, after 90 min, chambers were washed with Buffer L and then incubated for 30 min with Buffer L and 1:300 diluted antibody (Invitrogen 17H2L9). Chambers were then washed with Buffer L prior to imaging in Buffer L with oxygen scavenger system (above). For real-time colocalization assays, slides were prepared as follows: On the microscope, 100 μl WCE spiked with oxygen scavenger system was added to flow chamber via pipetting followed by immediate image acquisition.

Single molecule TIRFM colocalization assays image collection and analysis

All images were collected on a Nikon TE-2000 inverted TIRF microscope with a 100 \times oil immersion objective (Nikon Instruments) with an Andor iXon X3 DU-897 EMCCD camera. Images were acquired at 512 px \times 512 px with a pixel size of 0.11 $\mu\text{m}/\text{px}$ at 10 MHz. Atto-647 labeled CEN DNAs were excited at 640 nm for 300 ms, GFP-tagged proteins were excited at 488 nm for 200 ms, and mCherry-tagged proteins were excited at 561 nm for 200 ms. For endpoint colocalization assays, single snapshots of all channels were acquired. For real-time colocalization assays, images in 561 nm channel and 488 nm channel were acquired every 5 s with acquisition of the DNA-channel (647 nm) every 1 min for 45 min total (541 frames) using Nikon Elements acquisition software. Snapshots were processed in a CellProfiler 4 image analysis (Stirling *et al.*, 2021) pipeline using RelateObjects module to determine colocalization between DNA channel (647 nm) and GFP (488 nm) and mCherry (561 nm) channels. Results were quantified and plotted using MATLAB (The Mathworks, Natick, MA). Adjustments to example images (contrast, false color, etc.) were made using FIJI (Schindelin *et al.*, 2012) and applied equally across entire field of view of each image.

For real-time colocalization assay, a custom-built image analysis pipeline was built in MATLAB (R2019b) to extract DNA-bound intensity traces for the different fluorescent species, to convert them into ON/OFF pulses and to generate the empirical survivor function data. First, the image dataset was drift-corrected using either fast Fourier Transform cross-correlations or translation affine transformation depending on the severity of the drift. DNA spots were identified after binarizing the DNA signal using global background value as threshold, as well as size and time-persistence filtering. Mean values of z-normalized fluorescent markers intensities were measured at each DNA spot at each time frame, and local background was subtracted. Z-normalized traces were then binarized to ON/OFF pulses by applying a channel-specific, manually adjusted threshold value unique to all traces in a given image set. Pulse onsets, durations and overlaps between channels were then derived. For plotting clarity, z-normalized traces shown in the figures were zero-adjusted so that the baseline signal lies around zero. Pulses in ON state at the end of the image acquisition (right censored) were annotated and included as unweighted in lifetime estimates. Kaplan–Meier analysis and log rank tests were performed in MATLAB (R2021a). Adjustments to example plot images (contrast) as well as generation of example plot source movies were made using FIJI (Schindelin *et al.*, 2012).

Statistical tests

Right-censored lifetimes were included in an unweighted Kaplan–Meier analysis to estimate survival functions, censored events typically comprised $< 5\%$ of observed lifetimes. Survival functions including 95% confidence intervals were plotted using KMplot (Curve Cardillo, 2008) and *P*-values for comparing the Kaplan–Meier survival plots are provided in the figure legends and were computed using the log-rank test within Logrank (Cardillo, 2008). Different lifetime plots were considered significantly different with a *P*-value less than 0.05. Significance between off-rates were determined by two-tailed unpaired *t*-tests.

Data availability

Custom software written in MATLAB (R2021a) was used for TIRF colocalization residence lifetime analysis and plot generation. The source code is publicly available at <https://github.com/FredHutch/Automated-Single-Molecule-Colocalization-Analysis>. All primary datasets and associated data used for analysis in all figures are available at Zenodo, <https://zenodo.org/> and assigned the identifier (10.5281/zenodo.7939301). All primary data reported in this paper will be shared by the lead contact upon request.

Expanded View for this article is available [online](#).

Acknowledgements

All imaging was performed at the Fred Hutchinson Cancer Center Cellular Imaging Core (supported by the Fred Hutch/University of Washington Cancer Consortium P30 CA015704), and we thank Jin Meng and Lena Schroeder for their experimental help. We also thank members of the SB and CLA labs for critical reading of the manuscript. ARP was supported by postdoctoral fellowship NIH F32GM136010. JDL was supported by CVP training grant 5T32HL7312-39 and a Washington Research Foundation Fellowship Award. CLA was supported by NIH R01GM079373 and R35GM134842. SB was supported by NIH R01GM064386 and is also an investigator of the Howard Hughes Medical Institute.

Author contributions

Andrew R Popchock: Conceptualization; resources; data curation; software; formal analysis; funding acquisition; validation; investigation; visualization; methodology; writing – original draft; project administration; writing – review and editing. **Joshua D Larson:** Conceptualization; funding acquisition; methodology; writing – review and editing. **Julien Dubrulle:** Conceptualization; resources; data curation; software; formal analysis; visualization; writing – review and editing. **Charles L Asbury:** Conceptualization; resources; data curation; formal analysis; supervision; funding acquisition; investigation; visualization; methodology; project administration; writing – review and editing. **Sue Biggins:** Conceptualization; resources; formal analysis; supervision; funding acquisition; investigation; visualization; methodology; writing – original draft; project administration; writing – review and editing.

Disclosure and competing interests statement

The authors declare that they have no conflict of interest.

References

- Aitken CE, Marshall RA, Puglisi JD (2008) An oxygen scavenging system for improvement of dye stability in single-molecule fluorescence experiments. *Biophys J* 94: 1826–1835
- Aravamudhan P, Felzer-Kim I, Joglekar AP (2013) The budding yeast point centromere associates with two Cse4 molecules during mitosis. *Curr Biol* 23: 770–774
- Baker RE, Rogers K (2005) Genetic and genomic analysis of the AT-rich centromere DNA element II of *S. cerevisiae*. *Genetics* 171: 1463–1475
- Bensasson D, Zarowiecki M, Burt A, Koufopanou V (2008) Rapid evolution of yeast centromeres in the absence of drive. *Genetics* 178: 2161–2167
- Beutel BA, Gold L (1992) *In vitro* evolution of intrinsically bent DNA. *J Mol Biol* 228: 803–812
- Biggins S (2013) The composition, functions, and regulation of the budding yeast kinetochore. *Genetics* 194: 817–846
- Bobkov GOM, Huang A, van den Berg SJW, Mitra S, Anselm E, Lazou V, Schunter S, Feederle R, Imhof A, Lusser A et al (2020) Spt6 is a maintenance factor for centromeric CENP-A. *Nat Commun* 11: 2919
- Cai M, Davis RW (1990) Yeast centromere binding protein CBF1, of the helix-loop-helix protein family, is required for chromosome stability and methionine prototrophy. *Cell* 61: 437–446
- Camahort R, Li B, Florens L, Swanson SK, Washburn MP, Gerton JL (2007) Scm3 is essential to recruit the histone H3 variant Cse4 to centromeres and to maintain a functional kinetochore. *Mol Cell* 26: 853–865
- Carbon J (1984) Yeast centromeres: structure and function. *Cell* 37: 351–353
- Carbon J, Clarke L (1984) Structural and functional analysis of a yeast centromere (CEN3). *J Cell Sci Suppl* 1: 43–58
- Cardillo G (2008) LogRank: comparing survival curves of two groups using the log rank test. <http://www.mathworks.com/matlabcentral/fileexchange/22317>
- Cheeseman IM (2014) The kinetochore. *Cold Spring Harb Perspect Biol* 6: a015826
- Cho US, Harrison SC (2011a) Ndc10 is a platform for inner kinetochore assembly in budding yeast. *Nat Struct Mol Biol* 19: 48–55
- Cho US, Harrison SC (2011b) Recognition of the centromere-specific histone Cse4 by the chaperone Scm3. *Proc Natl Acad Sci USA* 108: 9367–9371
- Clarke L, Carbon J (1985) The structure and function of yeast centromeres. *Annu Rev Genet* 19: 29–56
- Cleveland DW, Mao Y, Sullivan KF (2003) Centromeres and kinetochores: from epigenetics to mitotic checkpoint signaling. *Cell* 112: 407–421
- Cole HA, Howard BH, Clark DJ (2011) The centromeric nucleosome of budding yeast is perfectly positioned and covers the entire centromere. *Proc Natl Acad Sci USA* 108: 12687–12692
- Crawford DJ, Hoskins AA, Friedman LJ, Gelles J, Moore MJ (2008) Visualizing the splicing of single pre-mRNA molecules in whole cell extract. *RNA* 14: 170–179
- Cumberledge S, Carbon J (1987) Mutational analysis of meiotic and mitotic centromere function in *Saccharomyces cerevisiae*. *Genetics* 117: 203–212
- Curve Cardillo G (2008) KMPLOT: Kaplan–Meier estimation of the survival function. <http://www.mathworks.com/matlabcentral/fileexchange/22293>
- Dechassa ML, Wyns K, Li M, Hall MA, Wang MD, Luger K (2011) Structure and Scm3-mediated assembly of budding yeast centromeric nucleosomes. *Nat Commun* 2: 313
- Dechassa ML, Wyns K, Luger K (2014) Scm3 deposits a (Cse4-H4)₂ tetramer onto DNA through a Cse4-H4 dimer intermediate. *Nucleic Acids Res* 42: 5532–5542
- Dendooven T, Zhang Z, Yang J, McLaughlin SH, Schwab J, Scheres SHW, Yatskevich S, Barford D (2022) Cryo-Em structure of the complete inner kinetochore of the budding yeast point centromere. *bioRxiv* <https://doi.org/10.1101/2022.12.12.520091> [PREPRINT]
- Dhatchinamoorthy K, Shivaraju M, Lange JJ, Rubinstein B, Unruh JR, Slaughter BD, Gerton JL (2017) Structural plasticity of the living kinetochore. *J Cell Biol* 216: 3551–3570
- Drew HR, Travers AA (1985) DNA bending and its relation to nucleosome positioning. *J Mol Biol* 186: 773–790
- Dunleavy EM, Roche D, Tagami H, Lacoste N, Ray-Gallet D, Nakamura Y, Daigo Y, Nakatani Y, Almouzni-Pettinotti G (2009) HJURP is a cell-cycle-dependent maintenance and deposition factor of CENP-A at centromeres. *Cell* 137: 485–497
- Filipescu D, Naughtin M, Podsypanina K, Lejour V, Wilson L, Gurard-Levin ZA, Orsi GA, Simeonova I, Toufektchan E, Attardi LD et al (2017) Essential role

- for centromeric factors following p53 loss and oncogenic transformation. *Genes Dev* 31: 463–480
- Foltz DR, Jansen LE, Bailey AO, Yates JR 3rd, Bassett EA, Wood S, Black BE, Cleveland DW (2009) Centromere-specific assembly of CENP-A nucleosomes is mediated by HJURP. *Cell* 137: 472–484
- Friedman LJ, Gelles J (2012) Mechanism of transcription initiation at an activator-dependent promoter defined by single-molecule observation. *Cell* 148: 679–689
- Friedman LJ, Chung J, Gelles J (2006) Viewing dynamic assembly of molecular complexes by multi-wavelength single-molecule fluorescence. *Biophys J* 91: 1023–1031
- Furuyama S, Biggins S (2007) Centromere identity is specified by a single centromeric nucleosome in budding yeast. *Proc Natl Acad Sci USA* 104: 14706–14711
- Furuyama T, Henikoff S (2009) Centromeric nucleosomes induce positive DNA supercoils. *Cell* 138: 104–113
- Gaudet A, Fitzgerald-Hayes M (1987) Alterations in the adenine-plus-thymine-rich region of CEN3 affect centromere function in *Saccharomyces cerevisiae*. *Mol Cell Biol* 7: 68–75
- Gkikopoulos T, Singh V, Tsui K, Awad S, Renshaw MJ, Scholfield P, Barton GJ, Nislow C, Tanaka TU, Owen-Hughes T (2011) The SWI/SNF complex acts to constrain distribution of the centromeric histone variant Cse4. *EMBO J* 30: 1919–1927
- Gordon DJ, Resio B, Pellman D (2012) Causes and consequences of aneuploidy in cancer. *Nat Rev Genet* 13: 189–203
- Guan R, Lian T, Zhou BR, He E, Wu C, Singleton M, Bai Y (2021) Structural and dynamic mechanisms of CBF3-guided centromeric nucleosome formation. *Nat Commun* 12: 1763
- Guo MS, Kawamura R, Littlehale ML, Marko JF, Laub MT (2021) High-resolution, genome-wide mapping of positive supercoiling in chromosomes. *Elife* 10: e67236
- Hedouin S, Logsdon GA, Underwood JG, Biggins S (2022) A transcriptional roadblock protects yeast centromeres. *Nucleic Acids Res* 50: 7801–7815
- Herman JA, Toledo CM, Olson JM, DeLuca JG, Paddison PJ (2015) Molecular pathways: regulation and targeting of kinetochore-microtubule attachment in cancer. *Clin Cancer Res* 21: 233–239
- Hewawasam GS, Dhatchinamoorthy K, Mattingly M, Seidel C, Gerton JL (2018) Chromatin assembly factor-1 (CAF-1) chaperone regulates Cse4 deposition into chromatin in budding yeast. *Nucleic Acids Res* 46: 4440–4455
- Hinshaw SM, Harrison SC (2019) The structure of the Ctf19c/CCAN from budding yeast. *Elife* 8: e44239
- Holland AJ, Cleveland DW (2009) Boveri revisited: chromosomal instability, aneuploidy and tumorigenesis. *Nat Rev Mol Cell Biol* 10: 478–487
- Hornung P, Troc P, Malvezzi F, Maier M, Demianova Z, Zimniak T, Litos G, Lampert F, Schleiffer A, Brunner M et al (2014) A cooperative mechanism drives budding yeast kinetochore assembly downstream of CENP-A. *J Cell Biol* 206: 509–524
- Hoskins AA, Friedman LJ, Gallagher SS, Crawford DJ, Anderson EG, Wombacher R, Ramirez N, Cornish VW, Gelles J, Moore MJ (2011) Ordered and dynamic assembly of single spliceosomes. *Science* 331: 1289–1295
- Joglekar AP, Bouck DC, Molk JN, Bloom KS, Salmon ED (2006) Molecular architecture of a kinetochore-microtubule attachment site. *Nat Cell Biol* 8: 581–585
- Joglekar AP, Bouck D, Finley K, Liu X, Wan Y, Berman J, He X, Salmon ED, Bloom KS (2008) Molecular architecture of the kinetochore-microtubule attachment site is conserved between point and regional centromeres. *J Cell Biol* 181: 587–594
- Kixmoeller K, Allu PK, Black BE (2020) The centromere comes into focus: from CENP-A nucleosomes to kinetochore connections with the spindle. *Open Biol* 10: 200051
- Kunkel GR, Martinson HG (1981) Nucleosomes will not form on double-stranded RNA or over poly(dA).poly(dT) tracts in recombinant DNA. *Nucleic Acids Res* 9: 6869–6888
- Lacoste N, Woolfe A, Tachiwana H, Garea AV, Barth T, Cantaloube S, Kurumizaka H, Imhof A, Almouzni G (2014) Mislocalization of the centromeric histone variant CenH3/CENP-A in human cells depends on the chaperone DAXX. *Mol Cell* 53: 631–644
- Lang J, Barber A, Biggins S (2018) An assay for *de novo* kinetochore assembly reveals a key role for the CENP-T pathway in budding yeast. *Elife* 7: e37819
- Larson JD, Hoskins AA (2017) Dynamics and consequences of spliceosome E complex formation. *Elife* 6: e27592
- Larson JD, Rodgers ML, Hoskins AA (2014) Visualizing cellular machines with colocalization single molecule microscopy. *Chem Soc Rev* 43: 1189–1200
- Leber V, Nans A, Singleton MR (2018) Structural basis for assembly of the CBF3 kinetochore complex. *EMBO J* 37: 269–281
- Liebl K, Zacharias M (2021) Accurate modeling of DNA conformational flexibility by a multivariate Ising model. *Proc Natl Acad Sci USA* 118: e2021263118
- Longtine MS, McKenzie A 3rd, Demarini DJ, Shah NG, Wach A, Brachat A, Philippsen P, Pringle JR (1998) Additional modules for versatile and economical PCR-based gene deletion and modification in *Saccharomyces cerevisiae*. *Yeast* 14: 953–961
- Lowary PT, Widom J (1998) New DNA sequence rules for high affinity binding to histone octamer and sequence-directed nucleosome positioning. *J Mol Biol* 276: 19–42
- Mahlke MA, Nechemia-Arbely Y (2020) Guarding the genome: CENP-A-chromatin in health and cancer. *Genes* 11: 810
- McAinsh AD, Marston AL (2022) The four causes: the functional architecture of centromeres and kinetochores. *Annu Rev Genet* 56: 279–314
- McGrew J, Diehl B, Fitzgerald-Hayes M (1986) Single base-pair mutations in centromere element III cause aberrant chromosome segregation in *Saccharomyces cerevisiae*. *Mol Cell Biol* 6: 530–538
- McKinley KL, Cheeseman IM (2016) The molecular basis for centromere identity and function. *Nat Rev Mol Cell Biol* 17: 16–29
- Melters DP, Bradnam KR, Young HA, Telis N, May MR, Ruby JG, Sebra R, Peluso P, Eid J, Rank D et al (2013) Comparative analysis of tandem repeats from hundreds of species reveals unique insights into centromere evolution. *Genome Biol* 14: R10
- Miller MP, Asbury CL, Biggins S (2016) A TOG protein confers tension sensitivity to kinetochore-microtubule attachments. *Cell* 165: 1428–1439
- Mizuguchi G, Xiao H, Wisniewski J, Smith MM, Wu C (2007) Nonhistone Scm3 and histones CenH3-H4 assemble the core of centromere-specific nucleosomes. *Cell* 129: 1153–1164
- Murphy MR, Fowlkes DM, Fitzgerald-Hayes M (1991) Analysis of centromere function in *Saccharomyces cerevisiae* using synthetic centromere mutants. *Chromosoma* 101: 189–197
- Musacchio A, Desai A (2017) A molecular view of kinetochore assembly and function. *Biology* 6: 5
- Nishimura K, Fukagawa T, Takisawa H, Kakimoto T, Kanemaki M (2009) An auxin-based degron system for the rapid depletion of proteins in nonplant cells. *Nat Methods* 6: 917–922
- Palmer DK, O'Day K, Trong HL, Charbonneau H, Margolis RL (1991) Purification of the centromere-specific protein CENP-A and demonstration that it is a distinctive histone. *Proc Natl Acad Sci USA* 88: 3734–3738

- Pinsky BA, Tatsutani SY, Collins KA, Biggins S (2003) An Mtw1 complex promotes kinetochore biorientation that is monitored by the Ipl1/Aurora protein kinase. *Dev Cell* 5: 735–745
- Popchock AR, Tseng KF, Wang P, Karplus PA, Xiang X, Qiu W (2017) The mitotic kinesin-14 KlpA contains a context-dependent directionality switch. *Nat Commun* 8: 13999
- Popchock AR, Jana S, Mehl RA, Qiu W (2018) Engineering heterodimeric kinesins through genetic incorporation of noncanonical amino acids. *ACS Chem Biol* 13: 2229–2236
- Prunell A (1982) Nucleosome reconstitution on plasmid-inserted poly(dA) · poly(dT). *EMBO J* 1: 173–179
- Ranjitkar P, Press MO, Yi X, Baker R, MacCoss MJ, Biggins S (2010) An E3 ubiquitin ligase prevents ectopic localization of the centromeric histone H3 variant via the centromere targeting domain. *Mol Cell* 40: 455–464
- Santaguida S, Musacchio A (2009) The life and miracles of kinetochores. *EMBO J* 28: 2511–2531
- Schindelin J, Arganda-Carreras I, Frise E, Kaynig V, Longair M, Pietzsch T, Preibisch S, Rueden C, Saalfeld S, Schmid B et al (2012) Fiji: an open-source platform for biological-image analysis. *Nat Methods* 9: 676–682
- Sehnal D, Bittrich S, Deshpande M, Svobodová R, Berka K, Bazgier V, Velankar S, Burley SK, Koča J, Rose AS (2021) Mol* Viewer: modern web app for 3D visualization and analysis of large biomolecular structures. *Nucleic Acids Res* 49: W431–W437
- Sheltzer JM, Blank HM, Pfau SJ, Tange Y, George BM, Humpton TJ, Brito IL, Hiraoka Y, Niwa O, Amon A (2011) Aneuploidy drives genomic instability in yeast. *Science* 333: 1026–1030
- Shrestha RL, Ahn GS, Staples MI, Sathyan KM, Karpova TS, Foltz DR, Basrai MA (2017) Mislocalization of centromeric histone H3 variant CENP-A contributes to chromosomal instability (CIN) in human cells. *Oncotarget* 8: 46781–46800
- Shukla M, Tong P, White SA, Singh PP, Reid AM, Catania S, Pidoux AL, Allshire RC (2018) Centromere DNA destabilizes H3 nucleosomes to promote CENP-A deposition during the cell cycle. *Curr Biol* 28: e3924
- Stirling DR, Swain-Bowden MJ, Lucas AM, Carpenter AE, Cimini BA, Goodman A (2021) CellProfiler 4: improvements in speed, utility and usability. *BMC Bioinformatics* 22: 433
- Stoler S, Rogers K, Weitze S, Morey L, Fitzgerald-Hayes M, Baker RE (2007) Scm3, an essential *Saccharomyces cerevisiae* centromere protein required for G2/M progression and Cse4 localization. *Proc Natl Acad Sci USA* 104: 10571–10576
- Stormberg T, Lyubchenko YL (2022) The sequence dependent nanoscale structure of CENP-A nucleosomes. *Int J Mol Sci* 23: 11385
- Struhl K, Segal E (2013) Determinants of nucleosome positioning. *Nat Struct Mol Biol* 20: 267–273
- Sullivan KF, Hechenberger M, Masri K (1994) Human CENP-A contains a histone H3 related histone fold domain that is required for targeting to the centromere. *J Cell Biol* 127: 581–592
- Widom J (2001) Role of DNA sequence in nucleosome stability and dynamics. *Q Rev Biophys* 34: 269–324
- Wisniewski J, Hajji B, Chen J, Mizuguchi G, Xiao H, Wei D, Dahan M, Wu C (2014) Imaging the fate of histone Cse4 reveals *de novo* replacement in S phase and subsequent stable residence at centromeres. *Elife* 3: e02203
- Xiao H, Mizuguchi G, Wisniewski J, Huang Y, Wei D, Wu C (2011) Nonhistone Scm3 binds to AT-rich DNA to organize atypical centromeric nucleosome of budding yeast. *Mol Cell* 43: 369–380
- Yan K, Zhang Z, Yang J, McLaughlin SH, Barford D (2018) Architecture of the CBF3-centromere complex of the budding yeast kinetochore. *Nat Struct Mol Biol* 25: 1103–1110
- Yan K, Yang J, Zhang Z, McLaughlin SH, Chang L, Fasci D, Ehrenhofer-Murray AE, Heck AJR, Barford D (2019) Structure of the inner kinetochore CCAN complex assembled onto a centromeric nucleosome. *Nature* 574: 278–282
- Yatskevich S, Muir KW, Bellini D, Zhang Z, Yang J, Tischer T, Predin M, Dendooven T, McLaughlin SH, Barford D (2022) Structure of the human inner kinetochore bound to a centromeric CENP-A nucleosome. *Science* 376: 844–852
- Zhou BR, Yadav KNS, Borgnia M, Hong J, Cao B, Olins AL, Olins DE, Bai Y, Zhang P (2019) Atomic resolution cryo-EM structure of a native-like CENP-A nucleosome aided by an antibody fragment. *Nat Commun* 10: 2301
- Zhou N, Shi L, Shan S, Zhou Z (2021) Molecular basis for the selective recognition and ubiquitination of centromeric histone H3 by yeast E3 ligase Psh1. *J Genet Genomics* 48: 463–472



License: This is an open access article under the terms of the [Creative Commons Attribution](https://creativecommons.org/licenses/by/4.0/) License, which permits use, distribution and reproduction in any medium, provided the original work is properly cited.